A review of the second normal-stress difference; its importance in various flows, measurement techniques, results for various complex fluids and theoretical predictions

O Maklad and R J Poole✉

School of Engineering, University of Liverpool, Liverpool, L69 3GH, UK

Abstract

Shear flow is ubiquitous. Not only is it arguably the most widely-used deformation type to characterise complex fluids in rheological studies but also, in practice, the deformation most likely to occur in the great majority of flows, e.g. involving fluid transport through pipes or conduits. In steady simple shear flow the rheological properties of a complex fluid are completely characterised in just three material functions; the variation with shear rate of the shear viscosity and the so-called first and second normal-stress differences. Despite requiring only three material functions to be completely characterised, most shear-flow rheological characterisations are usually restricted simply to the shear viscosity and, at best, the variation of the first normal-stress difference N_1 with shear rate. The second normal-stress difference N_2 remains very much neglected. For dilute polymer solutions where this quantity may be negligibly small in comparison to the first normal-stress difference, such neglect is justified but for a whole range of complex fluids – indeed even polymer solutions outside of the dilute regime and especially melts – it is not clear that N_2 may be safely disregarded. Indeed, in this review article we spotlight a number of flows where second normal-stress differences are of importance and potentially major consequence. Following this attention, we review the many experimental techniques which have been proposed for its measurement and survey the available literature for measurements of this quantity for various complex fluids including the aforementioned polymeric solutions, melts, liquid crystals, dense non-Brownian suspensions (both with Newtonian and complex fluid bases), semi-dilute wormlike micellar fluids and magnetorheological fluids. Theoretical predictions for N_2 from various commonly-used continuum constitutive equations – primarily from the polymer literature – are also given and their asymptotic predictions at low and high shear rates compared. Finally, we end with a brief summary and outlook.

KEYWORDS: normal-stresses, viscoelastic fluids, shear flow, secondary flow

✉robpoole@liv.ac.uk, + 44 151 794 4806

1. Introduction

Knowledge of a material's rheological properties is essential in understanding how such a material will respond under flow. Given the potential complexity of the material response, understanding of the rheological behaviour is usually built up via exposure to different types of kinematics, e.g. steady, transient and/or oscillatory, for different types of deformation. By far the most prevalent rheological characterisation is so-called "steady simple shear flow" where the resulting material response is then characterised completely by just three steady-state material functions; the shear viscosity (η) and the so-called first (N_1) and second (N_2) normal-stress differences. Note, for an incompressible fluid it is not possible to measure all three total normal stresses (i.e. $\tau_{xx} + p$, $\tau_{yy} + p$ and $\tau_{zz} + p$) because the pressure (p) is an undefined dynamical variable and therefore that is why only two normal-stress *differences* are required in which case the pressure cancels and then $N_1 = \tau_{xx} - \tau_{yy}$ and $N_2 = \tau_{yy} - \tau_{zz}$. These quantities are defined in **Figure 1** which provides a schematic of these stresses acting on streamlines in a homogeneous shear flow in a Cartesian coordinate system for various contributions of N_1 and N_2. For example materials which exhibit positive N_1 and negligible N_2 the resulting normal stress distribution is equivalent to an extra *tension* along the streamlines (i.e. lines everywhere parallel to the velocity vector), with an isotropic state of stress in planes normal to the streamlines (Barnes, Hutton, and Walters, 1989, p59). Despite this ubiquity of steady shearing in the rheological canon, often the material characterisation is restricted to a simple determination of the variation of the shear viscosity with shear rate and, far less frequently, the variation of the first normal-stress difference with shear rate. In comparison, the second normal-stress difference has received far less attention and is rarely measured. One may conjecture the reasons for this neglect but a primary reason may be that for one of the most studied viscoelastic fluids – namely polymer solutions – it is well known that N_2 is much smaller than N_1 and is therefore often "safely" neglected for most problems: in fact, in the dilute limit, most theoretical predictions give precisely $N_2 = 0$ yet, as we shall show, for polymeric melts and solutions in the concentrated and/or entangled regimes $N_2 \sim -0.1 - 0.3\, N_1$. A secondary reason is undoubtedly that experimental measurements of N_2 are non-trivial. Finally, we note that the recent intense interest in dense suspensions of non-colloidal particles, where it is has been found that N_2 is the significant normal-stress difference and larger than N_1, has, to a degree, reinvigorated the techniques to measure N_2 that were originally proposed for polymeric systems. In so doing, these studies have shown the importance, and value, of not simply neglecting this property based on results for other complex fluid systems

where it is indeed negligible (namely dilute polymeric solutions). We believe there are many other complex fluids, for example emulsions, foams, surfactant solutions in different phases outside of wormlike etc, where a knowledge of the second-normal stress difference is limited or non-existent, which could equally benefit from measurements of this property.

Despite this neglect, there are numerous situations when the second normal-stress difference can give rise to interesting fluid dynamic behaviour which can, in turn, lead to important effects. For example in laminar fully-developed axisymmetric duct flow with a constant cross-sectional area – such as in circular pipe flow or annular flow between two concentric circles – in the governing momentum equation only the shear viscosity is important and the normal-stress differences play no role aside from modifying the pressure – with, as highlighted in **Figure 1**, N_1 forming a tension along streamlines and N_2 forming a tension along vortex lines in the cross-sectional plane (i.e. tangential to the velocity vector). As soon as axisymmetry is broken however, for example by making the duct elliptic in cross-section (Green and Rivlin, 1956), square (Townsend, Walters, and Waterhouse, 1976), triangular or even more complex tear-duct shaped (Letelier, Acosta, Córdova, et al., 2002) extended to arbitrary domain shapes in (Siginer and Letelier, 2011) or through an eccentric annulus (Letelier, Siginer, Almendra, et al., 2019; Mollica and Rajagopal, 1999), gradients of N_2 then *may* drive a secondary motion which is entirely absent for Newtonian fluids under the same conditions (for the unconvinced reader this is nicely explained in the short paper by Speziale, 1984). **Figure 2** highlights various results from the literature which show the complex forms these secondary flows may take for different cross-sections/boundary conditions. This secondary motion, although significantly weaker in magnitude than the streamwise velocity, nevertheless has important applications in enhancing mixing and heat transfer significantly above the equivalent rectilinear flow (Gao and Hartnett, 1996; Siginer and Letelier, 2010) and in certain polymer processing such as wire coating (Tadmor and Bird, 1974). Such secondary-flow effects have been well studied numerically (Debbaut, Avalosse, Dooley, et al., 1997; Gervang and Larsen, 1991; Townsend et al., 1976; Xue, Phan-Thien, and Tanner, 1995; Yue, Dooley, and Feng, 2008) and, to a lesser extent, experimentally (Debbaut et al., 1997; Gervang and Larsen, 1991). Although most works on this topic consider polymeric flows, such N_2-driven secondary flows have also been observed for dense non-colloidal suspensions (A. Ramachandran and Leighton, 2008; Zrehen and Ramachandran, 2013). The topic of secondary flows driven by second normal-stress difference in polymeric systems is nicely reviewed in Siginer, 2011.

The secondary flows just discussed in fully-developed duct flow arise due to a breaking of axisymmetry in the geometry: they are absent in pipe flow (i.e. circular cross section) or axial flow through a concentric annulus (i.e. flow in the circular space between two circles) and necessarily in flow in an infinitely wide channel (i.e. pressure-driven flow between parallel plates). Even in these geometries second normal-stress difference effects can be observed by essentially breaking the symmetry of the boundary conditions and "cutting" the geometry in half, thus making the flow "open" to the atmosphere i.e. gravity driven open channel flow or through a semi-circular trough (Tanner, 1970; Wineman and Pipkin, 1966). The resulting free surface deforms due to the variation in N_2 caused by the tension along vortex lines in the perpendicular cross-sectional plane, as the shear rate at the free surface varies from a maximum at the wall (due to the no-slip condition) to zero at the centreline of the duct (due to symmetry). A concave surface should be observed when N_2 is positive, while a negative N_2 leads to a convex shape similar to that shown in **Figure 3** for a polymer solution. Put simply, a negative N_2 leads to compression in the vortex lines in a plane perpendicular to the flow direction. This compressive stress is maximum at the wall where the shear rate is maximum and zero at the centreline due to symmetry. At equilibrium, the stress component normal to the surface must be equal to the atmospheric pressure. Thus, the surface lifts at the centre to provide a hydrostatic pressure to balance this difference and takes on a convex shape. For positive N_2 the rationale is opposite and the free surface dips at the centre as the height of the fluid at the wall is pinned by the contact line. Under the assumption that the free surface deflection is small and no secondary flow occurs such that the base flow remains viscometric, this "tilted trough" approach has been proposed to measure N_2 and has been successfully used to determine that N_2 is negative and linearly proportional to the modulus of the shear stress for dense non-colloidal suspensions of spheres for example (Couturier, Boyer, Pouliquen, et al., 2011; Dai, Bertevas, Qi, et al., 2013). Full non-linear simulations of such tilted trough experiments would be interesting to determine how significant the secondary flow driven by N_2 is in these cases and its effect on the use of the free surface as a "pressure gauge". Study of the related pressure-driven flow in "partially full" pipe flows, hitherto restricted solely to Newtonian fluids (Guo and Meroney, 2013; Ng, Cregan, Dodds, et al., 2018), would also prove fruitful in this regard as the second normal-stress difference will drive secondary flows in such flows much as has been observed for "full" non axisymmetric duct flows (discussed above).

Another situation where the second normal-stress difference is of vital importance is in limiting accurate rheological measurements using cone-and-plate and parallel-plate devices where, beyond a certain shear rate, the free surface where the fluid sample meets the outside

air destabilizes. This is now commonly referred to as "edge facture" (or shear fracture) and results in the normally curved meniscus of the free surface splitting into two, one enclosing a collar of liquid on the rotating cone or plate and the other enclosing a bank on the stationary plate as shown in **Figure 4** (Hutton, 1963). The problem has been well studied for a variety of fluid systems, primarily polymeric (Inn, Wissbrun, and Denn, 2005; Lee, Tripp, and Magda, 1992) but also in suspensions of dense non-colloidal spheres (Sui and McKenna, 2007; Tanner and Dai, 2019; Zarraga, Hill, and Leighton, 2000) and more complex fluids such as commercial toothpastes (Keentok and Xue, 1999). Recognising the importance of the second normal-stress difference on this instability Tanner and co-workers (Tanner and Keentok, 1983 and Keentok and Xue, 1999) predicted it to occur for a critical magnitude $|N_2(\dot{\gamma})| > \sigma/\delta$ of the second normal-stress difference N_2 in the fluid, given a surface tension σ of the fluid-air interface and an assumed geometrical length scale δ (often taken to be the gap). Although this criterion has been shown to be correct from a phenomenological point-of-view (Huilgol, Panizza, and Payne, 1993), it was not until the recent work of Fielding and co-workers (Hemingway and Fielding, 2019; Hemingway, Kusumaatmaja, and Fielding, 2017) that a better understanding of the instability was provided, see **Figure 4(c)**. The role of the second normal-stress difference – more precisely the rate of change of N_2 with shear rate – remains key to the edge fracture phenomena.

One of the most unexpected effects in non-Newtonian fluid mechanics is the so-called "rod climbing" or Weissenberg effect where, when a rotating rod is placed in a container of an elastic fluid such as a viscous dilute polymeric solution, the liquid climbs the rod as shown in **Figure 5(a)**. The driving mechanism for the effect is usually explained as being driven via a tension from N_1 in the curved streamlines near to the rod which produces a hoop stress squeezing the liquid inwards. As a consequence, the free surface rises until the additional hydrostatic pressure pushing outwards balances the hoop stress squeezing inwards. However, as the classic analysis of Beavers and Joseph, 1975 for a second order fluid shows, the effect is actually proportional to a combination of both normal-stress differences (for a second order fluid: $N_2 + 0.25\, N_1$). For dilute polymeric solutions, where N_1 is positive and N_2 negligible, this produces a positive value of this quantity and the fluid climbs the rod. In contrast for dense suspensions of non-colloidal spheres, N_2 is negative and significantly larger than N_1 (which is also negative) leading to "rod dipping" as shown in **Figure 5(b)** (Boyer, Pouliquen, and Guazzelli, 2011; Hinch, 2011). As we will discuss in Section 2, much like the tilted trough, some researchers have made use of this rod-climbing (or rod *dipping*) experiment to measure N_2.

Although it is well known that for a variety of viscoelastic constitutive models that a jump in the first normal stress difference N_1 across an interface drives an interfacial instability in, for example two-layer Couette flow (Renardy, 1988) or co-extrusion channel flows (Wilson and Rallison, 1997), it is also the case that the second normal-stress difference may drive related instabilities. For such "layered" fluids, Renardy and Renardy, 1998 demonstrated that when material properties of the layer fluids are chosen such that there is no N_1 jump at the interface (i.e. the flow should be stable), that a jump in the second normal-stress difference across the interface can lead to 3D instabilities. Brady and Carpen, 2002 showed that, more generally, fluids with a negative second normal stress difference can be unstable with respect to transverse or spanwise perturbations and illustrated this general result for two-layer Couette and falling film flows of viscous suspensions of noncolloidal particles. A similar N_2 effect could also be responsible for fibre coating instabilities (Hinch, 2020), and there is an obvious link to the driving mechanisms for edge fracture discussed above.

In microfluidic flows, second normal-stress differences may also be important. For example, in the important area of "particle focusing" using viscoelastic fluids to induce particle separations in microfluidic devices, Villone, D'Avino, Hulsen, et al., 2013 predicted numerically that the secondary-flow known to occur in square duct flow alters the migration scenario for spherical particles as shown in **Figure 6(a)**. Feng, Magda, and Gale, 2019 showed experimentally that N_2 may induce multiple stream focusing phenomenon and enable an approach for manipulating the particle trajectory and separation of particles in a microchannel, see **Figure 6(b)**.

In creeping flows of viscoelastic liquids in curved pipes, where it is known that the first normal-stress difference can induce a secondary flow, it has been shown that the second normal stress difference can drastically suppress the secondary flow and, in the case of small curvature ratios, make the flow approximate the corresponding Poiseuille flow in a straight pipe (Fan, Tanner, and Phan-Thien, 2001)

Finally, a negative second normal-stress difference has been shown theoretically (Avagliano and Phan-Thien, 1998; Beris, Avgousti, and Souvaliotis, 1992; Shaqfeh and Larson, 1992) to have a strong stabilisation regarding the onset of so-called purely elastic instabilities in flows of viscoelastic fluids with streamline curvature (McKinley, Pakdel, and Öztekin, 1996; Shaqfeh, 1996).

Having demonstrated in this introduction the wide range of flows where the second normal-stress difference is of importance, the subject of the remainder of this current review is as follows. In section 2 we survey the different approaches – some already alluded to – that have been proposed in the literature for the experimental determination of N_2. We follow this in section 3 by collecting together reliable data available in the literature for N_2: primarily this is for polymeric solutions and melts, but also includes liquid crystals, dense non-Brownian suspensions (both with Newtonian and complex fluid bases), semi-dilute wormlike micellar fluids and magnetorheological fluids. In section 4 theoretical predictions for N_2 from various commonly-used continuum constitutive equations – from the polymer literature – are also given and their asymptotic predictions at low and high shear rates compared. Finally, in section 5, we end with a brief summary and outlook.

2. Methods of measuring the second normal-stress difference N_2

In this section, the different techniques that have been proposed in the literature for measuring N_2 will be discussed in detail supported by schematic diagrams to illustrate the technique used and the resulting equations necessary to determine N_2 from the measured quantities. In the following section this is complemented with some previous results from the literature to highlight the sign, magnitude and scaling with shear rate/stress of this quantity. The various measurement methods have been developed in the last five decades or so and, although consistent trends can be observed among the different fluid systems, such measurements are still far from routine and each approach has its own limitations. Therefore, one of the main purposes of this work is to gather all the methods in one place together with a succinct description of their practical implementation. Given the well-known problems, and incorrect data obtained, when using pressure tappings to measure the pressure in viscoelastic fluids (the so-called "hole pressure error" (Broadbent, Kaye, Lodge, et al., 1968; Tanner and Pipkin, 1969)) – to be explained in detail in Section 2.10 – we will largely restrict our overview to papers that do not use such pressure tappings and avoid discussion of many early papers which did not recognise the importance of this effect.

2.1 Cone-and-plate & parallel-plate thrust (CP-PP$_T$)

The variation of the first normal-stress difference with shear rate (i.e. $N_1(\dot{\gamma})$) can usually (Barnes et al., 1989; Whorlow, 1992) be measured directly with any standard rheometer fitted

with a force rebalance transducer with high normal-force sensitivity and resolution, using the normal thrust on the cone (or the plate) in a standard small angle cone-and-plate geometry, shown schematically in **Figure 7(a)**, according to:

$$N_1(\dot{\gamma})=\frac{2F_{CP}(\dot{\gamma})}{\pi R^2} \quad (1)$$

where F_{CP} is the axial thrust on a cone of radius R and $\dot{\gamma}=\frac{\omega}{\alpha}$ is the homogeneous shear rate, where ω is the angular velocity and α is the cone angle. Although deceptively simple, we note the derivation, and the attendant assumptions inherent in this derivation, are rather subtle and we refer the interested reader to the excellent discussion in Morozov and Spagnolie, 2015 for a detailed description of the derivation of Eqn. 1. For viscometric flow between parallel plates, shown in **Figure 7(b)**, the axial thrust on either of the plates is related to the difference between the first and second normal-stress differences according to:

$$N_1(\dot{\gamma})\text{-}N_2(\dot{\gamma}_R)=\frac{2F_{PP}(\dot{\gamma}_R)}{\pi R^2}\left(1+\frac{1}{2}\frac{d\,lnF_{PP}(\dot{\gamma}_R)}{d\,ln\dot{\gamma}_R}\right) \quad (2)$$

where F_{PP} is the axial thrust on a plate of radius R and $\dot{\gamma}_R=\frac{\omega R}{h}$ is the shear rate at the edge and h is the plate separation. The second normal-stress difference - at a given shear rate - can then be obtained by subtracting the two results. It was assumed in the derivation of the last two equations that the sample at the free surface is either perfectly spherical (Eqn. 1) or cylindrical (Eqn. 2) with no edge fracture and the radial normal-stress component τ_{rr} is equal to the ambient pressure (Bird, Armstrong, and Hassager, 1987; Ginn and Metzner, 1969; Kotaka, Michio, and Mikio, 1959). It should also be noted that, practically, subtracting two values which have nearly equal values leads to significant uncertainty in the value of N_2 (and, potentially, even the sign of this quantity). There is also a fundamental difference between the cone-and-plate geometry, where the shear rate is uniform and the flow-field homogeneous, and the parallel-plate geometry where the flow field is non-homogenous and the shear rate varies from zero at the axis of rotation to a maximum at the rim ($\dot{\gamma}_R$). Thus, caution is necessary when using this method to measure small values of N_2. In experimental practice, inertia and/or secondary flows reduce the measured axial thrust and several analytical studies have attempted to take this effect into consideration in the following closed form (Barnes et al., 1989):

$$\Delta F=0.075\,\pi\rho\omega^2R^4 \quad (3)$$

where ΔF (N) is the correction to the thrust measurement required at a specific shear rate, ρ is the fluid density in kg/m^3, ω is the rotational velocity of the cone or the plate in rad/s and R is

radius of the cone or the plate in m. By reducing the plate separation (h) it is possible to obtain the same shear rate at lower rotation speeds and this approach can be used to reduce inertial effects (subject to care being taken to avoid errors in the gap height (Davies and Stokes, 2005)). In addition to the inertia correction, normal-force transducer "drift" can also be problematic in obtaining accurate data, although protocols can be developed to attempt to "correct" such effects via post processing, see e.g. Casanellas, Alves, Poole, et al., 2016 or Poole, 2016. Surface tension and the wetting characteristics of materials used for the surfaces (i.e. the contact angle of the free surface makes with solid surfaces) have also been shown to have potentially important effects on the measurement of the total thrust in parallel-plate devices (Hutton, 1972). Thus, although the combination of cone-and-plate and parallel-plate measurements for the determination of N_2 appears relatively straightforward via Eqns. 1 and 2, the practical challenges in determining repeatable quantitative data are significant. For relatively dilute polymeric solutions for example, the forces associated with the inertia *corrections* used to determine N_1 can often be larger in magnitude than the *actual measurement*, see e.g. Zilz, Schäfer, Wagner, et al., 2014.

2.2 Cone-and-plate with distance adjustment (CPD_T)

In this method a cone-plate geometry is used but, in contrast to the classical situation where the apex of the cone should just (not) physically contact the plate, the gap h is systematically varied (in practice even in classical cone-plate flow the cone is often "truncated" to avoid potential damage). As in the previous method, the first normal-stress difference is measured from the axial thrust on the cone at the truncation gap (h~0) according to Eq. (4):

$$N_1(\dot{\gamma}) = \frac{2F(\dot{\gamma})}{\pi R^2} \qquad \text{at } h\sim 0 \qquad (4)$$

where $F(\dot{\gamma})$ is the axial thrust at a given apparent shear rate $\dot{\gamma} = \dot{\gamma}_{ap} = \frac{\omega}{\alpha}$ which needs to be varied such that the rate of change of $N_1(\dot{\gamma})$ with shear rate can be accurately determined, ω is the angular velocity of the rotating cone and α is the angle of the gap (it is an "apparent" shear rate as the shear rate is only truly this in the limit $h = 0$). Following these initial measurements, a number of additional measurements of the axial thrust, at constant apparent shear rate, are made for the cone raised to different heights h, which allow the calculation of the "apparent" normal-stress difference N_{ap} and its change with the adjusted height, **Figure 7(c)**:

$$N_{ap}=\frac{2F(h)}{\pi R^2} \qquad \text{at } h\neq 0 \qquad (5)$$

where $F(h)$ is the axial thrust when varying the cone-plate distance (at constant apparent shear rate). Knowledge of the rate of change of first normal-stress difference with shear rate coupled with the rate of change of the apparent normal-stress difference with distance h, the second normal-stress difference can then be calculated accordingly:

$$N_2(\dot{\gamma})=-\dot{\gamma}.\frac{dN_1(\dot{\gamma})}{d\dot{\gamma}}-\frac{R\ \tan\alpha}{2}.\frac{dN_{ap}(h)}{dh}\Bigg|_{\dot{\gamma}_{ap}=constant\ \&\ at\ the\ limit\ h=0} \qquad (6)$$

This method was first presented by Jackson and Kaye, 1966 and then was further developed by Marsh and Pearson, 1968 and Rautenbach, Schümmer, and Petersen, 1975 – with the improvement shown in Eq. (7) – in order to avoid error amplification involved with differentiation of both N_1 and N_{ap}:

$$N_1(\dot{\gamma}_R)-\left(1-\frac{\dot{\gamma}_R}{\dot{\gamma}_{ap}}\right).N_2(\dot{\gamma})=N_{ap}\left(\dot{\gamma}_R,\dot{\gamma}_{ap}\right)\times\left\{1+\left(1-\frac{\dot{\gamma}_R}{\dot{\gamma}_{ap}}\right)\cdot\frac{\partial\log N_{ap}\left(\dot{\gamma}_R,\dot{\gamma}_{ap}\right)}{2\cdot\partial\log\dot{\gamma}_R(\dot{\gamma}_{ap}=constant)}\right\} \qquad (7)$$

where $\dot{\gamma}_R=\frac{R\omega}{h+R\alpha}$ is the shear rate at the rim of the cone (i.e. at the sample edge). The variable gap cone/plate does not appear to have been used much, most likely due to the sensitivity to the differentiation needed in Eq. (7).

2.3 Cone-and-plate or parallel-plate with pressure gradient (CP_G or PP_G)

In contrast to the previous methods discussed, which involve taking numerous measurements with different geometries or gap heights, if not just the total thrust on the plate can be measured but also the *pressure gradient* in the set up then measurements of N_2 can be made more reliably. This method relies on measuring the local pressure distribution on the plate in the shear flow of the cone-and-plate or the parallel-plate geometry, **Figure 7(d)** (Christiansen and Leppard, 1974; Magda, Lou, Baek, et al., 1991; Ohl and Gleissle, 1992). From the angular momentum conservation in a cone-and-plate geometry, a relationship between N_2 and the pressure distribution on the cone can be derived (Bird et al., 1987):

$$-\Pi_{\theta\theta}(r)\ -\ P_a=\ -(N_1+2N_2)\cdot\log(r/R)-N_2 \qquad (8)$$

where $\Pi_{\theta\theta}(r)$ is the local pressure acting on the plate and P_a is the atmospheric pressure and their sum is the net pressure force exerted by the sample on the cone at a specific radial position r (where R is again the radius of the cone). This relationship predicts a linear relationship between the local pressure on the cone and the logarithm of radial position ratio. Thus if the local pressure is plotted against this logarithm the data should be a straight line of slope -(N_1+2N_2) and, if this straight line is extrapolated to the rim of the cone (r=R), the local net pressure should equal -N_2 as shown in the inset of **Figure 8(a)** (Magda, Lou, et al., 1991). To obtain the most reliable data, it appears to be better to avoid this extrapolation to estimate N_2 but rather to use the *slope* of the data. In this case, N_1 needs to be calculated first e.g. from the total axial thrust on the cone using Eq. (1). The same assumptions of the sample being spherical at the edges with no edge fracture and the radial normal stress equal to the ambient pressure P_a still apply to this method and therefore the same practical difficulties as mentioned previously hold. However, the benefits of this single-measurement approach over the approaches outlined in Sections 2.1 and 2.2 cannot be overstated. The downside is that current commercial rheometers do not provide local pressure measurement capability and therefore bespoke devices (Baek and Magda, 2003) need to be made using flush-mounted pressure transducers (as already noted, pressure tappings usually used for such purposes in Newtonian fluids are not suitable for viscoelastic fluids).

In the case of the shear flow between parallel plates the equivalent relationships are (Ohl and Gleissle, 1992; Singh and Nott, 2003):

$$N_1(\dot{\gamma}_R)+N_2(\dot{\gamma}_R)=\left(\frac{d\,\Pi_{\theta\theta}(r=0)}{d\,ln\dot{\gamma}_R}\right)_{PP} \tag{9}$$

$$-N_2(\dot{\gamma}_R)=\Pi_{\theta\theta}(r=R)-P_a \tag{10}$$

2.4 Cone-and-partitioned-plate (CPP)

The study of Meissner, Garbella, and Hostettler, 1989 following Pollett, 1955 developed a "cone-and-partitioned-plate" method to avoid the experimental obstacles in measuring the local pressure distribution and to reduce the effect of edge fracture and other potential instabilities. The plate in the cone-and-plate geometry is replaced by a smaller central stem of radius R_i and surrounded by an outer ring of outer radius R_o which is equal to the cone radius, as shown in **Figure 7(e)**. The normal force is only detected on the inner stem and the outer ring is fixed to the rheometer. The annular gap between the stem and the ring is designed

to be very small (typically ~0.05 mm) (Meissner et al., 1989). By using samples with different radii R, where $R_i \leq R \leq R_o$, the radial variation of the pressure can be deduced and the ratio of the normal force on the stem to the total force exerted by the whole sample F_i/F can be calculated. This enables N_2 to be calculated from Eq. (11) after obtaining N_1 on the full sample in a separate cone-and-plate measurement with $R \leq R_o$ using Eq. (1):

$$\frac{F_i\, R^2}{F\, R_i^{\,2}} = 1 + 2\left(1 + 2\frac{N_2}{N_1}\right) \cdot \ln\frac{R}{R_i} \tag{11}$$

Bird et al., 1987; Schweizer, 2002; Snijkers and Vlassopoulos, 2011 developed Eq. (11) into another form to calculate the apparent normal-stress difference N_{app} as shown in Eq. (12), such that $N_{app} = N_1$ if $R = R_{stem}$.

$$N_{app} = \frac{2F\,(\dot{\gamma})}{\pi R_i^{\,2}} = N_1 + 2\,(N_1 + 2N_2) \cdot \ln\frac{R}{R_i} \tag{12}$$

where N_{app} is the apparent value of N_1 calculated from the axial thrust on the inner stem of radius R_i, and R is the radius of the sample which is estimated from the mass (m), density (ρ) of the sample and the cone angle (θ) as follows:

$$R = \sqrt[3]{\frac{3m}{2\pi\rho\theta}} \tag{13}$$

From the linear relationship implied in Eq. (12), plotting N_{app} against $\ln\frac{R}{R_i}$, N_1 is obtained from the intercept and N_2 from the slope (i.e. 2 (N_1+2N_2)), an example is shown in **Figure 8(b)**, where $-\frac{N_2}{N_1} = 0.06$ (Schweizer, 2002). Unfortunately, this procedure has to be undertaken for every shear rate involving multiple measurements and multiple samples. On the other hand, using different stems on the same sample with radius R, enables measurements over a wide temperature range and on samples with different volumes which is important for measurements for some fluids e.g. polymer melts (Costanzo, Ianniruberto, Marrucci, et al., 2018). In this way, two apparent normal stresses are measured for every stem as shown in Eqs. (14), (15):

$$N_{app,1} = \frac{2F_1\,(\dot{\gamma})}{\pi R_1^{\,2}} = N_1 + 2\,(N_1 + 2N_2) \cdot \ln\frac{R}{R_1} \tag{14}$$

$$N_{app,2} = \frac{2(F_1 + F_2)\,(\dot{\gamma})}{\pi R_2^{\,2}} = N_1 + 2\,(N_1 + 2N_2) \cdot \ln\frac{R}{R_2} \tag{15}$$

The only two unknowns in these two equations are N_1 and N_2, which therefore can be obtained when both apparent forces are known at a given shear rate. This method also requires two different samples to perform the measurement for each stem. Schweizer and Schmidheiny, 2013 have presented the design of a cone-and-plate with three partitions (CPP3) to avoid the requirement to use different samples. In this design, an inner partition with radius R_1 to measure F_1, a middle partition with radius R_2 to measure F_2, and the outer partition is fixed to the rheometer to prevent edge fracture at high shear rates. The calculations follow the exact same procedure following Eqs. (14), (15).

2.5 Cone-and-ring or plate-and-ring (CR or PR)

In this "ring" method, an air bubble is trapped between a cone or a plate and a narrow ring as shown in **Figures 7(f), (g)**. The air bubble internal pressure P_C and the axial thrust F_{CR} or F_{PR} on the ring is measured to calculate N_2 directly from Eq. (16) or (17) (Harris, 1968; Ohl and Gleissle, 1992; van Es, 1974):

$$N_2 = -\frac{P_C}{2\,ln(R_1/R_2)} - \frac{F_{CR}}{\pi\left({R_2}^2 - {R_1}^2\right)} \qquad \text{Cone-and-ring} \quad (16)$$

$$N_2 = -P_C - \frac{1}{\pi}\frac{\partial F_{PR}}{\partial {R_1}^2} + \frac{R_1}{2}\frac{\partial P_C}{\partial R_1} \qquad \text{Plate-and-ring} \quad (17)$$

where R_1 and R_2 are the internal and external radii of the ring. As can be seen, the analysis when using the plate is much more complicated than the cone approach and multiple measurements must be taken using rings with different internal radii R_1 . It is essential, in using both methods, to ensure that no edge fracture happens at the inner or outer edges of the ring (Ohl and Gleissle, 1992).

One can see that generally using these various cone or plate approaches using a rheometer (i.e. those detailed in Sections 2.1-2.5) one faces a dilemma: a "simple" integral measurement technique to obtain, e.g. a "thrust", often requires multiple independent experiments followed up subtraction of two quantities of nearly equal magnitude, or differentiation of this experimental data with respect to various other parameters, or one makes recourse to a much more complicated experimental arrangement where pressure gradients (or numerous thrust measurements) can directly be measured. As Section 3 will show, where we discuss

experimental results for various systems, the pressure gradient approach seems the most robust and user-friendly method but outside of a few groups (Magda and Baek, 1994; Magda, Baek, DeVries, et al., 1991; Magda, Lou, et al., 1991) does not seem to have been more broadly adopted.

2.6 Rod climbing (Weissenberg effect) (RC)

As already discussed in the introduction, one of the famous and most convincing illustrations of the elasticity of polymeric fluids is the rod-climbing experiment, where the free surface climbs a thin rotating rod in a cylindrical container. This observation is commonly referred to as the "Weissenberg effect" following his early pioneering work on the topic (Weissenberg, 1947). In general, the free surface deflection in a rod-climbing experiment is sensitive to elasticity, inertia and normal stresses in the fluid and by analysing the equations of motion for a second order fluid, the free surface deflection can be approximately related to the fluid material functions in shear flow (Bird et al., 1987; Joseph and Beavers, 1977; Magda, Lou, et al., 1991). By taking into account surface tension and fluid inertia, Eq. (18) relates the height of the fluid free surface at the rod $h(\omega)$ and the rod angular velocity ω considering the rod diameter to be small enough compared to the diameter of the container to reduce inertial effects, **Figure 9(a)**:

$$h(\omega) = h_s + \frac{4R_1 \beta \omega^2}{2\sqrt{\rho g}\,(4\sqrt{\sigma} + R_1\sqrt{\rho g})} \qquad (18)$$

where h_s is the static free surface height at $\omega = 0$, R_1 is the rod radius, β is the so-called "climbing constant" (equal to $\frac{1}{2}\frac{N_1}{\dot{\gamma}^2} + 2\frac{N_2}{\dot{\gamma}^2}$), ρ is the fluid density, σ is the fluid surface tension, and g is the acceleration due to gravity. From this equation the climbing constant β can be calculated if the change of the free surface height with the angular speed can be accurately measured and, by measuring N_1 independently e.g. using a different rheometric technique, N_2 can be determined accordingly. This method appears to be simple, however care should be taken to the assumptions made when deriving Eq. (18). It was assumed that the measurements are in the "second order fluid" flow regime which strictly restricts measurements to low rotation/shear rates and the use of a different geometry and separate measurement to determine N_1 is another strong limitation, since it may involve extrapolation to shear rates that could not be measured in either of the two geometries. The use of exact relationships between the storage

modulus (G') measured in small amplitude oscillatory shear (SAOS) flow as the angular velocity (ω) tends to zero and the limiting behaviour of N_1 at vanishing shear rates $\left.\frac{G'(\omega)}{\omega^2}\right|_{\omega\to 0} = \left.\frac{N_1(\dot{\gamma})}{2\dot{\gamma}^2}\right|_{\dot{\gamma}\to 0}$ could be useful in this regard given the high accuracy with which SAOS measurements can usually be conducted. Another approach would be to use an intriguing empirical rule which seems to show that for some concentrated polymeric solutions and melts the first normal stress difference can be determined from the steady shear viscosity (Sharma and McKinley, 2012).

Joseph and Beavers, 1977 also discuss the ideal of a "normal stress amplifier" for the rod-climbing experiment where a layer of viscoelastic liquid is floated on top of another immiscible Newtonian liquid of different density. The normal stresses push the viscoelastic fluid up into the air and down into the less dense fluid. Hence, inertia and normal stresses are in conflict at the viscoelastic-air interface and in concert at the Newtonian-viscoelastic interface. This configuration can be regarded as a "normal stress amplifier" because the down-climb can be arbitrarily amplified by making the density difference at the lower interface very small and such differences can be "spectacular".

In contrast to the above approach, Boyer et al., 2011 derived the relation of the free surface deflection in a different manner for dense non colloidal suspensions. By solving the mass and momentum equations of a suspension with a Newtonian matrix, they developed Eqs. (19) & (20) assuming no inertia or surface tension effects:

$$h(r) = -h_0 \frac{R_1^2}{r^2} + h_1 \tag{19}$$

$$\rho g h_0 = -\left(\alpha_2 + \frac{1}{2}\alpha_1\right)\tau \tag{20}$$

where $h(r)$ is the free surface deflection at a specific radius r from the centre of the rod, R_1 is the rod radius, h_0 is obtained from fitting the experimental free surface profiles of the change of the free surface height with the radial position, and h_1 is a constant that can be determined from the mass conservation equation as shown in **Figure 8(c)**. By using h_0 in Eq. (20), the linear combination of normal-stress differences coefficients $\alpha_2 + \frac{1}{2}\alpha_1$ can be measured, where $\alpha_1 = \frac{N_1}{\tau}$ and $\alpha_2 = \frac{N_2}{\tau}$. As noted by Hinch, 2011, this differs from the classical perturbation

analysis of rod-climbing by Beavers and Joseph, 1975 discussed above who found the free surface is displaced upwards proportional to a certain combination of normal stresses (i.e. the "climbing constant" β referred to above) and varies in the radial direction as r^{-4}. This is the radial variation of the normal stresses, which are proportional to the square of the shear rate, which is the radial derivative of the $1/r$ flow. In contrast, suspensions of non-colloidal rigid spheres have normal stresses linearly proportional to the shear rate (rather than quadratically), and so the displacement of the free surface now varies as r^{-2}. There is therefore also a consequential change in the combination of the normal stresses to $N_2 + 0.5\ N_1$. Boyer et al., 2011 provided also surface tension and inertial correction terms to account for their effects. This method was proposed as being particularly suitable for dense noncolloidal suspensions where it is difficult to use rotational rheometry with small gaps due to the finite size of the particles as we will discuss more in Section 3. We note, however, that particle migration from regions of high shear rate to regions of low shear rate do affect rod climbing experiments for suspensions (see e.g. Boyer et al., 2011).

2.7 Tilted trough (TT)

As already discussed in the introduction, Wineman and Pipkin, 1966 studied the equations governing the flow down a straight tilted trough of arbitrary cross-section. In laminar fully-developed Newtonian flows, the free surface remains flat, while in viscoelastic flows, they postulated that the second normal-stress difference causes the free surface to either bulge upwards or deflect downwards in a concave or convex shape respectively depending on the sign of N_2. Without knowing of this analysis, the bulging of the surface in a rectangular channel was found experimentally (Tanner, 1970). Further work showed that much improved results could be obtained with a semi-circular trough filled to the brim (Fig 9b). This avoids the secondary flows in the rectangular trough and the cumbersome surface analysis of Couturier et al., 2011 needed to deal with the free surface (Dai et al., 2013; Dai, Qi, and Tanner, 2014). In this semi-circular trough the inclination angle can be used to determine the shear stress (via a force balance):

$$\tau(x) = \frac{1}{2}\rho g x \sin\alpha \qquad (21)$$

and the second normal-stress difference by measuring the free surface deflection $h(x)$

$$N_2(\tau_w) = \frac{\rho g}{\sin\alpha} \int_0^{\alpha} \sin\theta \; d(h_w \cos\theta) \qquad (22)$$

where ρ is the fluid density, g is the gravitational acceleration, x is the horizontal coordinate measured from the centre of the channel, α is the channel tilt angle as shown in **Figure 9(b)**, τ_w is the shear stress at the channel wall (i.e. $\tau_w = 0.5\rho g R_0 sin\alpha$), and h_w is the fluid free surface deflection at the wall where $x = R_0$. An experiment is then undertaken with fixed values of ρ, g and R_0 but the angle α is altered, so that the results are given as a table of h_w versus $sin\alpha$. Eq. (22) avoids subtraction between two values which is important for measuring small values of N_2 and it involves integration not differentiation which prevents unavoidable measurement error amplification, an example is shown in **Figure 8(d)** with the measurement error shown in grey (Tanner, 1970). The free surface was found to be concave and h_w is positive when N_2 is positive, while the free surface is convex and h_w is negative when N_2 is negative and this gives a clear indication on the sign of N_2 without recourse to any calculation. The analysis is correct to $O(h_w/R)$ if either the centre of the channel (as assumed in the analysis described above) or the edges are brought up to the diametral line. The latter is more convenient from an experimental perspective and then h_w needs to be replaced by h_0 (i.e. the height change at the channel centre rather than at the wall). The drawbacks of the trough technique are the (relatively) large volume of fluid required – being on the order of ~1 litre – and the range of shear stresses which can be probed being quite limited.

2.8 Cylindrical Couette shear cell

With the aim to measure first and second normal differences of small to moderate concentrated non colloidal suspensions, Singh and Nott, 2003 developed a cylindrical Couette shear cell method to overcome some of the difficulties using other techniques. In this method, the sample is sheared at a rate which is sinusoidal in time with constant frequency. **Figure 10(a)** shows a schematic diagram of the cylindrical Couette shear cell, it consists of an outer cup and an inner rotor with the sample being sheared in between. The radial normal stress τ_{rr} is measured on the outer stationary cup using a flush-mounted transducer located roughly midway between the base and the sample surface to avoid any end effects (see Davoodi, Lerouge, Norouzi, et al., 2018 for a detailed discussion of the effects of finite depth aspect ratio in cylindrical Couette flow;). The component of the stress which has the same frequency is then recorded using a lock-in amplifier eliminating error and signal noise (Singh and Nott,

2003). On the other hand, the axial normal stress τ_{zz} is measured on an identical sample but in a separate experiment using a parallel-plate and flush mounted transducer located at three radial positions on a stationary bottom plate as shown in **Figure 10(b)**, i.e. a similar setup explained to that in section 2.3. To prevent sample drainage, the top plate rotates over a pool containing the sample which may result in a non-viscometric flow near the rim (Bird et al., 1987). Using the radial and the axial components of the stress, the second normal-stress difference can be estimated from its definition (i.e. $N_2 = \tau_{rr} - \tau_{zz}$ in this coordinate system).

2.9 Flow birefringence

In the flow birefringence method, the full refractive index tensor is measured by projecting light beams along a number of intermediate paths oriented at independent angles between the normal and the shear flow directions as shown in **Figure 10(c)** (Brown, Burghardt, Kahvand, et al., 1995; Hongladarom and Burghardt, 1993). The sample is held between two prisms with faces cut at the same independent light path angles improving the ability to resolve the three independent stress components. A shear flow is imposed by translation of one of the prisms relative to the other. Subsequently, the birefringence is measured by a polarisation modulation technique (Frattini and Fuller, 1984; Olson, Brown, and Burghardt, 1998). This method is also sometimes referred to as "full tensor optical rheometry" (FTOR) which can also determine the time-dependent behaviour of N_2 which has not been widely reported because of the experimental difficulties with the various methods already discussed above (Kalogrianitis and van Egmond, 1997; Takahashi, Shirakashi, Miyamoto, et al., 2002).

2.10 Hole pressure error

As already discussed, any method which relies on measuring pressure via a hole in a bounding surface gives an incorrect result for viscoelastic fluids owing to the stretching of the streamlines as they pass over the hole. Where the streamlines are curved the normal stresses tend to "lift" the fluid out of the hole. This causes the pressure, p_H, measured by a transducer in the bottom of the hole to be lower than the pressure, p_1, measured by a flush-mounted transducer on the opposite wall. The resulting reduction in pressure ($\Delta p = p_1 - p_H$) has been shown theoretically – using a second-order fluid valid in the limit of slow and slowly varying flow – to be linearly related to the first normal stress difference and equal to (Tanner and Pipkin, 1969):

$$\Delta p = \frac{N_1}{4} \tag{23}$$

In general, as shown by Baird, 1975 or Malkus, Pritchard, and Yao, 1992 the relationship between the measured pressure difference and the normal stress differences can be used to determine *both* N_1 and N_2 if the "tapping"(slot) can be aligned transverse to the flow direction (Jensen and Christiansen, 2008; Kearsley, 1970):

$$N_1 = 2m\Delta p \tag{24}$$

and a separate tapping/slot can be aligned parallel to the flow direction:

$$-N_2 = -m\Delta p \tag{25}$$

where

$$m = \frac{d\ln(\Delta p)}{d\ln(\tau)} \tag{26}$$

The method does not seem to have been widely adopted – potentially due to unwanted flow being driven inside the tapping/slot in the flow-aligned/parallel case as highlighted by Baird (1976) – but has been used by Jensen and Christiansen, 2008 to estimate N_2 for a polymer melt. The topic is also nicely discussed in Tanner, 1988.

3. Second normal-stress difference results for various fluid systems

Section 3 will focus on the consistency of measurements of N_2 in general and the ratio $-\frac{N_2}{N_1}$ in particular for the various different fluid systems that are available in the literature. We will discuss results for dilute (Boger fluids), semi-dilute and concentrated polymer solutions together with polymeric melts and also limited results for different polymeric structure. Furthermore, "dense" suspensions of non-colloidal (i.e. unaffected by Brownian motion) particles in both Newtonian and viscoelastic base-fluid matrices will be discussed and how N_2 measurements vary with changes with particle concentration. Following discussion of these relatively well-studied systems, limited results for semi-dilute wormlike micellar solutions, liquid crystals and magnetorheological fluids will also be briefly addressed. An overview of data for all these systems is provided in **Table 1**.

3.1 Polymeric solutions and melts

Values of the normal-stress differences can be expected to change with the polymer concentration and solutions are classified into dilute, semi-dilute, and concentrated or, more generally, polymers can be studied in their melt form. Larson, 1988, p33 gives a nice explanation for the molecular origin of normal-stress differences in polymeric fluids as arsing from the distributions of polymer configuration. A positive N_1 implying more molecules are orientated in the flow direction in shear flow, whereas a negative N_2 implies that the orientation perpendicular to the shearing plane is depleted of polymer configurations relative to the orientation in the neutral direction.

A. Boger fluids/dilute polymer solutions

So-called "Boger" fluids are essentially solutions of dilute polymers in viscous solvents which then produce highly elastic fluids with nearly constant viscosity (as the polymeric contribution to the viscosity remains small any shear thinning therefore remains negligible Boger, 1977). In these model fluids in complex flows, elastic effects can then be separated from any viscous effects due to, for example, shear-thinning and these fluids have therefore found many important uses such as in studying purely elastic instabilities (James, 2009). It is usually assumed that second normal-stress differences in such Boger fluids, and dilute polymeric solutions in general, remain negligibly small. As a consequence, there are very few papers available in the literature which provide measurements of N_2 for Boger fluids and dilute solutions, in general, since such small values are typically below the resolution of many measurement techniques outlined in Section 2. Although limited to a maximum shear rate of ~60 s^{-1} (corresponding to a shear stress of 10 Pa) for their Boger fluid of a polyacrylamide (140 ppm) dissolved in maltose and water, Keentok, Georgescu, Sherwood, et al., 1980 did indeed report N_2 values close to zero using a tilted-trough approach. More recently, Dai et al., 2014, also using the tilted trough technique, found that N_2 was too small to measure for a Boger fluid comprised of corn syrup (by weight 79.42%), glycerin (19.8%), water (0.75%), and a small amount (300ppm) of a $5x10^6$ molecular weight polyacrylamide. Keentok and Tanner, 1982; Magda, Lou, et al., 1991 and Hu, Riccius, Chen, et al., 1990 studied an organic Boger fluid - the so-called 'M1' fluid - which consists of polyisobutylene dissolved in oligomeric polybutene with concentrations 0.1 and 0.24%, respectively. They reported $-\frac{N_2}{N_1} = 0.01$ and 0.11 ± 0.01,

respectively, with this difference being attributed to polymer concentration effects which most likely pushed the higher concentration solution out of the dilute regime and into the so-called concentrated un-entangled regime, as shown schematically in **Figure 11(a)**. Thus, the scant available data for dilute polymeric solutions (Boger fluids) indicates that, indeed, the second normal-stress difference in steady shear does seem to be negligibly small at roughly 1% of the value of the first normal-stress difference.

B. Semi-dilute and concentrated entangled solutions

To distinguish different concentration regimes, following Magda and Baek, 1994, we plot in **Figure 11(a)** a "phase diagram" for various concentrations and molecular weights using monodisperse polystyrene (PS) as an exemplar. To determine the extent of the dilute regime the so-called "critical overlap concentration" – which here we donate with the symbol c* - is determined from intrinsic viscosity measurements (Bird et al., 1987). In this regime the polymer chains are separated from each other and behave more or less independently, interacting primarily with the solvent molecules. Above c* the solutions are said to be semi dilute. At a higher concentration still, denoted c**, the solution enters a so- called concentrated regime in which each segment of the polymer chain does not have sufficient space available and separates semi-dilute from concentrated solutions based on the concentration and molecular weight of the polymer. Finally both semi dilute and concentrated solutions may be entangled or unentangled and c_E is used to demarcate unentangled from fully entangled solutions (Graessley, 1980; Magda and Baek, 1994). Magda and Baek measured the steady shear flow values of $-\frac{N_2}{N_1}$ for monodisperse PS solutions in the semidilute and concentrated entangled regimes and reported the same zero-shear rate value of 0.275 ± 0.005: they also reported that this ratio may shear thin to smaller values at higher shear rates. S. Ramachandran, Gao, and Christiansen, 1985 and Keentok and Tanner, 1982 observed a similar value of 0.29 and 0.31, respectively, for the ratio of $-\frac{N_2}{N_1}$ for a range of linear polymers but did not observe any shear thinning of this quantity at higher rates (potentially due to edge fracture restricting values of the maximum shear rate).

N_2 data for commonly-used commercial polymers in aqeuous solutions – such as a polyacrylamide (PAA) and polyethylene oxides (PEO) – appear to be quite rare. Keentok et al report values of N_2 = -0.065 - 0.1 N_1 with increasing concentrations (0.2-0.8% by weight) of a

PAA ("Separan AP 30") using the tilted-trough technique and similar values for PEO (WSR301) at 0.7 and 1% concentration. Assuming WSR301 has a molecular weight of 4 x 10^6 and following the approach outlined in Zilz et al., 2014 we get c*~550 ppm which would put these concentrations potentially into the concentrated regime. Christiansen and Leppard, 1974 using a cone-and-plate pressure gradient (CP_G) method for both a 3% PEO and a 2.5% PAA solution in more viscous water/glycerol solvents measured similiarly small values for N_2 being on the order of -0.1 N_1. It is somewhat surprising that there is so little second normal stress difference data for PEO and PAA fluids given their ubiquity in non-Newtonian fluid mechanics research but the limited data available suggests smaller values of N_2 than those measured for PS solutions in non-aqeuous solution. Limited data for polyisobuylene in various solvents – most like in the semi-dilute regime – also shows N_2 = -0.1-0.15 N_1.

This limited data for polymeric solutions would suggest that the second normal-stress difference - *outside* of the dilute regime - may be potentially significant and can be up to 30% of the first normal-stress difference. Despite such fluids being the most widely studied from a second normal-stress difference perspective, it is arguably the case that more data on aqeuous solutions would be welcome where molecular weight and concentration effects could be systematically investigated.

C. Polymer melts

Polymer melts are similar in many ways to concentrated entangled polymer solutions, but the difference between them being they are, so to speak, their "own" solvent. As a consequence, measurements for polymer melts have to occur at elevated temperatures (typically >50 ^oC). The second normal-stress differences in polymer melts has been found to be important to understand the onset of surface instability in rotational flows ("edge fracture" discussed in the introduction) and to reduce extrudate swell and sharkskin in extrusion flows (Costanzo et al., 2018; Schweizer, 2002). The most commonly used method to measure N_2 in polymer melts – virtually all data is for polystyrenes - is the cone-and-partitioned plate method (CPP) (described in Section 2.4) which was originally developed to overcome edge fracture instabilities and limited temperature measurement range (Costanzo, Huang, Iannirubertо, et al., 2016; Meissner et al., 1989; Schweizer, 2002; Snijkers and Vlassopoulos, 2011). The ratio of $-\frac{N_2}{N_1}$ for these polystyrene systems exhibits a shear-thinning behaviour, as also seen for a polyisoprene (Olson et al., 1998), it decreases from ~0.3 to ~0.1 at high shear rate (Costanzo

et al., 2018; Olson et al., 1998; Schweizer, Hostettler, and Mettler, 2008). This data for polystyrene melts is broadly consistent with data for concentrated polystyrene solutions.

D. Effect of polymer architecture

The study of S. Ramachandran et al., 1985 performed measurements on both linear concentrated polystyrene and branched "star" polybutadiene solutions to ascertain if polymer branching increase entanglement and hence affect N_2 values. They reported $-\frac{N_2}{N_1}$ ~0.29 for linear concentrated polymer solutions and 0.214 for all branched polymers studied with standard deviation of less than 2%. However, Lee, Magda, DeVries, et al., 1992 have also performed measurements on both linear and star polymer solutions and reported that star polymers with long and entangled branches enhances the value of $-\frac{N_2}{N_1}$ from 0.21 ± 0.01, for linear polymers, to 0.3 ± 0.01 for star polymers. Thus, the limited data available is not clear if polymer architecture has a significant effect, but once again highlights the significant uncertainty associated with measurements of N_2.

3.2 Liquid crystals

Liquid crystals may flow in a fluid-like manner, but also have the molecular alignment characteristics of a solid crystal and interesting optical properties. They consist of rod-like polymer solutions which align in parallel and exhibit crystallinity (Głowińska, Parcheta, and Datta, 2019; Wissbrun, 1981). These fluids can be isotropic solutions and their behaviour is broadly consistent with concentrated polymer solutions and $-\frac{N_2}{N_1} = 0.29 \pm 0.01$ (Baek, Magda, and Larson, 1993; Hongladarom and Burghardt, 1993; Magda, Baek, et al., 1991). However, the fully liquid-crystalline phase does exhibit some unique rheological behaviour. Magda, Baek, et al., 1991 found that the fluid pressure is below atmospheric at most locations in cone-and-plate shear flow with the lowest pressure happening at the cone tip. N_2 was found to be an oscillatory function of shear rate and its magnitude close to N_1 values with $-\frac{N_2}{N_1} > 0.5$. Moreover, N_2 was found to be positive in magnitude for a narrow shear rate range for specific polymer concentrations as shown in **Figure 11(b)**. The two methods used to measure N_2 for fully liquid crystalline fluids in the literature were CP_G and flow birefringence (Baek et al., 1993; Hongladarom and Burghardt, 1993; Magda, Baek, et al., 1991). Applying the rod-

climbing method on these fluids would be interesting as, if $N_2 \sim 0.5\, N_1$, this should result in rod *dipping* rather than rod climbing.

3.3 Non-Brownian suspensions

Suspensions, i.e. complex fluids composed of a mixture of solid particles and suspended in either Newtonian or non-Newtonian base fluids (referred to as the suspending "matrix" hereafter), exist in many natural and industrial applications. Non-Brownian suspensions refer to suspensions with particles typically much larger than a micron in radius therefore allowing thermal fluctuations to be neglected (Denn and Morris, 2014; Guazzelli and Pouliquen, 2018). Of course, it is not the particle size *per se* which is important in determining the relative importance of Brownian effects but rather the Péclet number – i.e. the characteristic rate for advection to that for diffusion and some of the data for such systems shown in **Table 1** is for smaller particles in more viscous solvents. Due to the relatively large particle size, standard cone-and-plate measurements are challenging due to particle jamming, potential non-continuum effects if the characteristic size of the geometry is on the same order as the particle and, additionally, edge fracture. As a consequence, most researchers studying suspensions prefer other methods over cone-and-plate, such as the rod-climbing method, cylindrical Couette, tilted trough, parallel-plates with pressure gradient or cone-and-plate with distance adjustment, as documented in **Table 1**.

A. Newtonian matrix suspensions

The available data is nicely reviewed in Guazzelli and Pouliquen, 2018 (see also Tanner, 2018) who demonstrate that, despite uncertainties and scatter across the various data sets, some concrete information for N_2 in such systems can be gleaned. Unlike polymeric solutions and melts where, as we have discussed, N_1 is positive and higher than N_2 which is negative, suspensions of spherical particles with a Newtonian matrix have been shown to exhibit the opposite behaviour with N_2 (still negative) but much higher than N_1 which in one study was found to be slightly positive Dbouk, Lobry, and Lemaire, 2013 and in others was found to be slightly negative (Denn and Morris, 2014). As already highlighted in the introduction, such "flipped" behaviour in comparison to polymers was clearly reported by Zarraga et al., 2000 and Boyer et al., 2011 using the rod-climbing method, instead of the free surface climbing up the rod, the suspension dips down near the rod. Both normal-stresses

differences have been shown to be linear in the modulus of the shear stress. The magnitude of the negative second normal-stress difference is seen to increase with increasing volume faction, growing especially quickly for volume concentrations (ϕ) greater than about 20% to reach a magnitude of roughly 40% of the shear stress at ϕ=50%. As discussed above, the properties of the first normal-stress difference have been the subject of more debate. The magnitude of N_1 seems unquestionably to be much smaller than that of N_2, but there was uncertainty regarding the sign. Most experiments found that N_1 was quite small and negative (Dai et al., 2013; Singh and Nott, 2003; Zarraga et al., 2000), while others report positive values (Dbouk et al., 2013; Gamonpilas, Morris, and Denn, 2016), and other studies that the value is too small to determine whether it is negative, positive or zero within experimental accuracy (Boyer et al., 2011; Couturier et al., 2011). The corrigendum of Gamonpilas, Morris, and Denn, 2018 which corrects an error in data reduction of their earlier study (Gamonpilas et al., 2016) and clarifies that N_1 is negative for their data leaves the study of Dbouk et al., 2013 as the only paper showing N_1 as positive: the consensus now seems to be that N_1 is indeed negative (Tanner, 2018). **Table 1** provides details for the actual ratios of $-N_2/N_1$, fluids and methods used in each of these studies.

B. Viscoelastic matrix suspensions

In contrast to Newtonian matrix suspensions, normal stresses for suspensions in a viscoelastic matrix appear at particle concentrations as low as 5% (Mall-Gleissle, Gleissle, McKinley, et al., 2002) and the rheology of such systems has recently been reviewed (Tanner, 2019). The ratio of $-\frac{N_2}{N_1}$ is seen to vary substantially between 0.1 and 1.6 and is potentially an effect of the viscoelastic matrix on the values of N_1, which was agreed to be positive among the different studies, unlike Newtonian suspensions where the sign of N_1 is still debated as discussed above (Aral and Kalyon, 1997; Haleem and Nott, 2009; Lin, Phan-Thien, and Cheong Khoo, 2014; Mall-Gleissle et al., 2002; Ohl and Gleissle, 1992; Zarraga, Hill, and Leighton, 2001), and highlighted in **Table 1**. Zarraga et al., 2001 performed rod climbing measurements for suspensions in a Boger fluid matrix and observed pure rod-climbing at low particle concentrations <30%, fluid dipping near the rod at high concentrations >50% and combined behaviour for intermediate concentrations with an upward climb near the rod and a downward deflection further away from the rod.

3.4 Wormlike micellar fluids

Micelles are formed by the self-assembly of surfactants in solution. Wormlike micelles or "living polymers" – so-called due to their rheological response being similar in many ways to polymer solutions – are a particularly interesting fluids because their long flexible cylindrical geometry can lead to entanglement even at relatively low concentrations (Rehage and Hoffmann, 1991). In semi-dilute solutions, wormlike micelles show remarkably simple rheological behaviour; their linear rheology measured in small amplitude oscillatory shear flow is often well described by a single-element Maxwell model with a single relaxation time. The non-linear rheological and flow response of wormlike micelles has proven to be incredibly rich and complex (Rothstein and Mohammadigoushki, 2020) and there are a large number of studies which investigate their shear rheological properties (e.g. Wheeler, Izu, and Fuller, 1996). Only two studies seem to have measured N_2 directly. J.-Y. Lee, Magda, Hu, et al., 2002 reported data for dilute surfactant solutions containing long, thin, wormlike micelles which undergo a shear-thickening transition at which the apparent viscosity jumps to a much higher value due to the formation of shear-induced structures. By averaging over a number of the dilute solution data sets and all the shear rates for which reliable data was obtained (using the CP_G technique where linear pressure profiles were observed), they obtained $-\frac{N_2}{N_1} = 0.16 \pm 0.005$. In contrast, Pipe, Kim, Vasquez, et al., 2010, using an identical technique, but for a semi-dilute entangled wormlike micelle, found $-\frac{N_2}{N_1} \sim 0.4$ but with significant uncertainty as the data is susceptibe to small variations in the fitted slope. Finally, Kim, Mewis, Clasen, et al., 2013 used a superposition of an oscillatory motion onto a steady-state shear flow to probe a semi dilute wormlike micellar solution. In this case the values for the normal stress components can also be obtained directly, without complex fitting procedures, from the in-phase superposition moduli. The data is consistent with a Giesekus model - to be described in the following section - such that $-\frac{N_2}{N_1} \sim 0.25$ in the low shear rate range. This the limited data obtained for semi dilute wormlike micelles would suggest that N_2 is at least as important as in concentrated and entangled polymeric solutions.

3.5 Magnetorheological fluids

Magnetorheological fluids are a special type of concentrated suspension of magnetisable particles suspended in a liquid matrix, when a magnetic field is applied to the

samples, the ferromagnetic particles form string-like structures parallel to the magnetic flux lines which can be used effectively in actuators, dampers, and clutches (Laun, Gabriel, and Schmidt, 2008). As a consequence of these magnetic-induced structures, normal-stress differences appear. Laun et al., 2008 measured N_1 and N_2 for magnetisable spherical carbonyl iron powder particles suspended in a hydrocarbon oil subjected to magnetic field with flux up to 1 T, using the CP-PP$_T$ method and found $-\frac{N_2}{N_1} \approx$ - 0.25 with both stress differences positive. In marked contrast in a theoretical study for such fluids - based on the assumption of equilibrium between hydrodynamic and magnetostatic torques and forces in a field-induced aggregate of particles subjected to shear - López-López, Kuzhir, Durán, et al., 2010, postulate that N_2 is negative and $-\frac{N_2}{N_1} \approx 0.17$. Such stark discrepancies about even the sign of the second normal-stress difference for these fluids suggest, in that age-old adage, more research is needed.

4. Material function predictions from common theoretical models

In this section we will provide predictions for the three material functions; $\eta(\dot{\gamma})$, $N_1(\dot{\gamma})$, and $N_2(\dot{\gamma})$ for a number of continuum models of the differential type and illustrate their behaviour. We start by presenting Oldroyd's "A", "B" and "co-rotational" models: although they can hardly be said to be commonly-used, the A and co-rotational models are included as they are arguably the simplest differential models that include a non-vanishing second-normal-stress difference in steady shear. We also consider more realistic models including the Giesekus model, the linear (non-simplified) Phan-Thien Tanner (PTT) model and the model due to Johnson-Segalman (JS). Our choice of constitutive equations is not meant to be exhaustive, rather illustrative. We also note more recent, microscopically-informed, equations for melts and concentrated polymeric solutions – such as the "pom pom" model (McLeish and Larson, 1998), the "Rolie-Poly" model (Likhtman and Graham, 2003) and the "GLaMM" (Graham, Likhtman and Milner, McLeish) model (Graham, Likhtman, McLeish, et al., 2003) predict a vanishing second normal-stress difference in steady shear (Holroyd, Martin, and Graham, 2017). An empirical modification to the pom pom model has been made to include non-zero N_2 by the addition of a "Giesekus-like" quadratic stress term, the so-called extended pom pom "XPP" model (Verbeeten, Peters, and Baaijens, 2001). Although the XPP model suffers from multiple solutions, admitting both positive and negative values of N_2 for example for fixed parameters (Inkson and Phillips, 2007), these can be avoided by restriction of the free

parameters to certain values (Baltussen, Verbeeten, Bogaerds, et al., 2010). Tanner and Nasseri, 2003 discuss the relationships between the XPP and the PTT family of models. Outside of the Oldroyd models, where they are included to demonstrate how this is done, we do not take into account solvent viscosity (/retardation time) effects and, for all models, restrict our analysis to isothermal, single-mode models (we note that such models are often inadequate in capturing the full complexity of real fluid behaviour). We also highlight the asymptotic behaviour of the material functions for the different models at both vanishingly small and high shear rates and document these in **Table 2**.

4.1 Oldroyd models

In his seminal paper, J G Oldroyd (Oldroyd, 1950) laid down the general foundations for deriving invariant forms "of rheological equations of state for a homogeneous continuum, suitable for application to all conditions of motion and stress". In so doing, he introduced his now-famous "convected" derivatives. To illustrate the power of the technique, he showed how it could be applied to differential equations of state for incompressible "elastico-viscous" type and picked a model due to Fröhlich and Sack, 1946, valid for small strains and written in a Cartesian coordinate system, but which now we would probably term a linear Jeffreys model (Bird et al., 1987; Morrison, 2001) :

$$\lambda_1 \frac{d\tau}{dt} + \tau = \eta \left(\dot{\gamma} + \lambda_2 \frac{d\dot{\gamma}}{dt} \right), \tag{24}$$

where λ_1 is the relaxation time, λ_2 is the retardation time (which is related to the relaxation time via the solvent η_2 and total viscosity $\eta = \eta_1 + \eta_2$ as $\lambda_2 = \frac{\eta_2}{\eta}\lambda_1$), τ the shear stress, $\dot{\gamma}$ the shear rate and *d*/*dt* the time derivative. Interestingly, Oldroyd discussed how there are an *infinite* number of possible sets of invariant equations of state which can be proposed for this model and then illustrated two possible invariant forms of this model, one which he called case "A" - which uses a lower convected derivative to make Eqn. 24 suitable for general flows - and case "B" which uses an upper convected derivative. In modern notation, these two models can be written as follows. For the Oldroyd-A model:

$$\lambda_1 \overset{\vartriangle}{\boldsymbol{\tau}} + \boldsymbol{\tau} = \eta(\dot{\boldsymbol{\gamma}} + \lambda_2 \overset{\vartriangle}{\dot{\boldsymbol{\gamma}}}) \tag{25}$$

and for the Oldroyd-B model

$$\lambda_1 \overset{\triangledown}{\boldsymbol{\tau}} + \boldsymbol{\tau} = \eta(\dot{\boldsymbol{\gamma}} + \lambda_2 \overset{\triangledown}{\dot{\boldsymbol{\gamma}}}) \tag{26}$$

where

$$\overset{\triangle}{\boldsymbol{\tau}} = \partial\boldsymbol{\tau}/\partial t + (\boldsymbol{u}.\nabla)\boldsymbol{\tau} + (\nabla\boldsymbol{u}).\boldsymbol{\tau} + \boldsymbol{\tau}.\nabla\boldsymbol{u}^{\boldsymbol{T}} \tag{27}$$

is the lower convected derivative and

$$\overset{\triangledown}{\boldsymbol{\tau}} = \partial\boldsymbol{\tau}/\partial t + (\boldsymbol{u}.\nabla)\boldsymbol{\tau} - \left(\nabla\boldsymbol{u}^{\boldsymbol{T}}\right).\boldsymbol{\tau} - \boldsymbol{\tau}.\nabla\boldsymbol{u} \tag{28}$$

is the upper convected derivative, $\boldsymbol{\tau}$ the stress tensor and $\dot{\boldsymbol{\gamma}} = \nabla\boldsymbol{u} + \nabla\boldsymbol{u}^{T}$ the strain rate tensor. Oldroyd then showed how, despite "at first sight these might appear to be trivially different generalizations", that in rotational Couette flow one model (the "Oldroyd-B") can give rise to the Weissenberg effect of rod climbing whilst the other, (the "Oldroyd-A") does not. This is because, despite both models exhibiting a constant shear viscosity, as **Table 2** shows, the Oldroyd-B model gives $N_1 \sim \dot{\gamma}^2 > 0$ and $N_2 = 0$ whereas the Oldroyd-A gives $N_1 \sim \dot{\gamma}^2 = -N_2$. As we discussed in the introduction, in the absence of inertia or surface tension in the slow flow limit, the Weissenberg effect is proportional to $(0.25\ N_1 + N_2)/\tau$ (Beavers and Joseph, 1975; Hinch, 2011) so that for the Oldroyd-B this term is positive $0.25\ N_1/\tau$, whereas for the Oldroyd-A it is of opposite sign and negative i.e. $-0.75\ N_1/\tau = 0.75\ N_2/\tau$.

As we have discussed, dilute polymeric solutions (and/or Boger fluids) do indeed exhibit a (nearly) constant shear viscosity and a positive N_1 which grows approximately quadratically with shear rate (James, 2009) the Oldroyd-B has proven, despite its simplicity, to be incredibly useful and has gone on to become, in many ways, the prototype, viscoelastic model. In contrast, surely due to the prediction of very high second normal-stress differences, the Oldroyd-A model has remained essentially unstudied. We note, however, how it is (arguably) the simplest model prediction that includes a non-zero N_2 and, as we show below, also that it represents the limiting low-shear rate behaviour for more complex models which do incorporate finite N_2. A model which acts as an intermediary between "A" and "B" is the so-called "co-rotational" Oldroyd (Oldroyd, 1958) which is:

$$\lambda_1\left(\frac{\overset{\vartriangle}{\boldsymbol{\tau}}}{2}+\frac{\overset{\triangledown}{\boldsymbol{\tau}}}{2}\right)+\boldsymbol{\tau}=\eta\left(\dot{\boldsymbol{\gamma}}+\lambda_2\left(\frac{\overset{\vartriangle}{\dot{\boldsymbol{\gamma}}}}{2}+\frac{\overset{\triangledown}{\dot{\boldsymbol{\gamma}}}}{2}\right)\right), \tag{29}$$

this model gives shear thinning of the shear viscosity, first and second normal-stress differences which grow quadratically at low shear rates but which plateau at high shear rates and a constant ratio of N_1=- 0.5N_2. Interest in the co-rotational Oldroyd (or co-rotational Maxwell) model has recently been reinvigorated due to it being the simplest possible constitutive equation for predicting the first, third, and fifth harmonics of the shear stress response in large amplitude oscillatory shear ("LAOS") see e.g. Giacomin, Bird, Johnson, et al., 2011 or Poungthong, Giacomin, Saengow, et al., 2019. We note that in the limit that the retardation time is set to zero, the Oldroyd-A is nothing but the so-called lower convected Maxwell (LCM) model, the Oldroyd-B the upper convected Maxwell (UCM) and the co-rotational Oldroyd, the co-rotational Maxwell (see e.g. Larson, 1988).

4.2 Giesekus model predictions

In an important paper Giesekus, 1982 developed a model which is ultimately nothing but a modified Oldroyd-B model but which now includes an additional quadratic term in stress:

$$\lambda\overset{\triangledown}{\boldsymbol{\tau}}+\boldsymbol{\tau}+\alpha\frac{\lambda}{\eta}\boldsymbol{\tau}\cdot\boldsymbol{\tau}=\eta\dot{\boldsymbol{\gamma}}, \tag{30}$$

the three material functions in shear are controlled by three parameters in the absence of solvent viscosity; a relaxation time, λ; the polymer viscosity, η, and the mobility factor α. In the absence of solvent viscosity (so $\lambda_2=\eta_2=0$ and therefore $\eta_1=\eta$ and $\lambda_1=\lambda$), the mobility factor must remain less than 0.5 to avoid a non-monotonic dependence of the shear stress on the shear rate for steady simple shear flow. Often this restriction is specifically relaxed to study fluids which may exhibit shear banding (Lerouge and Olmsted, 2020; Moorcroft and Fielding, 2014). The three material functions as a function of shear rate are given in Bird et al., 1987 and are therefore not unnecessarily repeated here. In the limit of no solvent viscosity, finite mobility factor and shear rate tending to infinity the following asymptotic formulae hold (Bird et al., 1987):

$$\eta(\dot{\gamma}) \sim \sqrt{\frac{(1-\alpha)}{\alpha}}\frac{\eta}{\lambda\dot{\gamma}} \tag{31}$$

$$N_1(\dot{\gamma}) \sim \frac{\sqrt{2}}{\alpha}\,(\alpha(1-\alpha))^{1/4}\frac{\eta\lambda\dot{\gamma}^2}{(\lambda\dot{\gamma})^{3/2}} \tag{32}$$

$$N_2(\dot{\gamma}) \sim -\frac{\eta\lambda\dot{\gamma}^2}{(\lambda\dot{\gamma})^2} \tag{33}$$

The complete predictions of the three normalised material functions; $\eta(\dot{\gamma})/\eta$, $N_1(\dot{\gamma}).\,\lambda/\eta$, and $N_2(\dot{\gamma}).\,\lambda/\eta$ are shown in **Figures 12(a)**, **(b)**, and **(c)** for different values of mobility factor α and **Figure 12(d)** shows the prediction of $-N_2/N_1$. We note that the material functions of the model due to Leonov (Leonov, 1976) are *identical* to the Giesekus model in steady simple shear flow when the mobility factor α =0.5 (Isaki and Takahashi, 2002) and are therefore encapsulated in the Giesekus predictions here presented.

4.3 Full Phan-Thien–Tanner (PTT) model predictions

We refer to this model as the "full" Phan-Thien and Tanner (PTT) model as often the simplified version of this model is more routinely used where the second normal-stress difference is identically zero (Alves, Oliveira, and Pinho, 2003). The PTT model was developed based on a temporary network theory by Phan-Thien, 1978; Phan-Thien and Tanner, 1977 and the networks of polymer chains are connected by junctions that constantly change their configuration. The model was originally proposed to capture the rheological behaviour of polymer melts (Alves, Pinho, and Oliveira, 2001) and is given as follows:

$$Y(\mathrm{Tr}\,\boldsymbol{\tau})\boldsymbol{\tau} + \lambda\overset{\square}{\boldsymbol{\tau}} = \eta\dot{\boldsymbol{\gamma}}, \tag{34}$$

$\overset{\square}{\boldsymbol{\tau}}$ is the so-called Gordon–Schowalter (GS) convected derivative defined as

$$\overset{\square}{\boldsymbol{\tau}} \cong \frac{D\boldsymbol{\tau}}{Dt} - \boldsymbol{\tau}\cdot\nabla u - \nabla u^T\cdot\boldsymbol{\tau} + \xi(\boldsymbol{\tau}\cdot\boldsymbol{D} + \boldsymbol{D}\cdot\boldsymbol{\tau}) \tag{35}$$

The parameter ξ accounts for the slip between the molecular network and the continuum medium (when $\xi = 0$ the GS convected derivative becomes simply Oldroyd's upper convective derivative and this represents the "simplified" form of the PTT model in which the second normal stress difference is zero in steady simple shear). $Y(\mathrm{Tr}\,\boldsymbol{\tau})$ is stress coefficient function which in general has an exponential form, but here we use the linearised stress coefficient function $f(\mathrm{Tr}\,\boldsymbol{\tau})$ given by

$$f(\mathrm{Tr}\,\boldsymbol{\tau}) = 1 + \frac{\varepsilon\lambda}{\eta}\mathrm{Tr}\,\boldsymbol{\tau} \qquad (36)$$

which was proposed in the original paper of Phan-Thien and Tanner, 1977, where ε is the upper limit to the extensional viscosity which is inversely proportional to it. If $\varepsilon = 0$, as a result, $f(\mathrm{Tr}\,\boldsymbol{\tau}) = 1$, which reduces exactly to the model due to Johnson and Segalman, 1977 described next. The three material functions as a function of shear rate are given explicitly in Alves et al., 2001 and are therefore not unnecessarily repeated here. The predictions of the normalised material functions are shown in **Figures 12(a)-(f)**.

4.4 Johnson-Segalman model

The Johnson-Segalman (JS) model (Johnson and Segalman, 1977) was developed to allow non-affine deformation of the molecular network junctions to occur:

$$\lambda\left(\left(1-\frac{a}{2}\right)\overset{\triangle}{\boldsymbol{\tau}} + \frac{a}{2}\overset{\triangledown}{\boldsymbol{\tau}}\right) + \boldsymbol{\tau} = \eta\dot{\boldsymbol{\gamma}}, \qquad (37)$$

the slip parameter a sets the relative importance of the two Oldroyd convected time derivatives described above and when this slip parameter is equal to 0 this corresponds to affine motion and the upper convected Maxwell model is recovered, and when this parameter is equal to 2 the lower convected Maxwell model recovered. As $a \to 1$, the model becomes the co-rotational Maxwell model (Goddard and Miller, 1966). In the original paper of Johnson and Segalman, 1977 they restricted $0 < a < 1$ ("because it is found that values of a in this range yield good results when compared with experiment"). We note that the JS model can also be expressed directly in terms of the GS convected derivative as $\boldsymbol{\tau} + \lambda\overset{\square}{\boldsymbol{\tau}} = \eta\dot{\boldsymbol{\gamma}}$ where a replaces ξ in Eqn 35. The three material functions as a function of shear rate are given in Barnes et al., 1989, p155 and are therefore not unnecessarily repeated here. With vanishingly small ε (= 0.001 say), the predictions of the normalised material functions are essentially the same as the linear PTT model with $a = \zeta$, if ε is larger the difference between the two models becomes more apparent as shown in **Figures 12 (e)**, and **(f)** especially for the shear viscosity but also for intermediate shear rates for N_1 and N_2 where the asymptotic behaviour at low and high shear rates remains identical (i.e. independent of ε) for these quantities.

4.5 Discussion of model predictions

Figure 12 shows the predictions for the various single-mode models and **Table 2** provides asymptotic expressions for the material functions at both vanishing small ($\lambda\dot{\gamma} \to 0$) and large ($\lambda\dot{\gamma} \to \infty$) non-dimensional shear rates. For these models – mainly proposed for polymer materials – the normal-stress difference responses of Oldroyd's models act as limiting cases for many of the other models. For example in the limit that the non-linear α parameter in the Giesekus model goes to zero and in the PTT and Johnson-Segalman (JS) models when $a=\xi=0$ (i.e. the Gordon Schowalter derivative simplifies to the upper convective), N_1 grows in all cases quadratically in shear rate and $N_2=0$ just as the Oldroyd B does. In the same small shear rate limit, but also in the limit that the non-linear parameters $\alpha=a=\xi \to 0$ but remains finite the models retain a small but finite N_2 which grows quadratically with shear rate and is directly proportional in magnitude to the finite non-linear parameters (i.e. α, a, or ξ). In the other "Oldroyd-A-like" limit, not shown in the plots, when α tends to 2 and $a=\xi=2$ both N_1 and $-N_2$ grow quadratically with shear rate and are equal in magnitude in this low shear rate limit. For other values of the non-linear parameters ($\alpha=1$, $a \to 1$ and $\xi \to 1$) the normal stress-differences of the co-rotational Maxwell model, viz N_1 growing quadratically and $N_2=-N_1/2$), are the more useful comparator. Although the various models exhibit quite similar behaviour in this low shear rate asymptote (which they must as the second order fluid response must be true in this slow-flow limit) both the shear viscosity outside of this limit and the normal-stresses exhibit different behaviour.

The normal-stress data for the various models, shown in **Figure 12(b)**, **(c)**, and **(f)** are normalised by the zero-shear rate elastic modulus (i.e. η/λ) and show that in the large shear rate limit the JS and PTT models become constants but the ratio of $-N_2/N_1$ for these models (shown in **Figure 12(d)**) remains constant for *all* shear rates. The Giesekus model shows subtly different behaviour with N_1 growing weakly with shear rate but $-N_2$ becoming constant. Thus, in the large shear rate regime, the ratio $-N_2/N_1$ shear thins for the Giesekus model. The predictions of N_2/N_1 (**Figure 12(d)**) in this high-shear rate limit would appear -as stated by Larson in his classic book dealing with polymeric constitutive equations (Larson, 1988, p120/121) - to offer a fairly sensitive test to discriminate between different constitutive equations. In particular, the Giesekus predictions that this ratio becomes vanishingly small whereas it remains fixed for the PTT and JS models.

The large shear rate asymptote of the non-linear elasticity of the models – estimated via a Weissenberg number defined as a ratio of the shear-rate dependent elastic stress N_1 to the shear-rate dependent viscous stress (i.e. $\eta(\dot{\gamma})\dot{\gamma}$) – shows that the Giesekus model grows like $\sim\lambda\dot{\gamma}^{0.5}$ whereas the JS and PTT models, due to the more intense shear-thinning shear viscosity, grow like $\sim\lambda\dot{\gamma}^{1}$ retaining the low-shear response. Thus, although N_1 normalised by the elastic modulus grows with shear rate in this high-shear limit for the Giesekus but *saturates* for the PTT and JS models, the Giesekus is "less elastic" in this limit as the actual viscous stress ($\eta(\dot{\gamma})\dot{\gamma}$) dominates more for this model than the other two. The differences between the JS and PTT models for different values of ε, shown in **Figure 12(f)**, are confined to a fairly narrow band of intermediate shear rates: the small and large shear rate asymptotic behaviour for the normal-stress differences being identical for the two models.

For a detailed description of other models and predictions of their N_2 response, we refer the interested reader to the excellent monograph of Larson, 1988. In particular the integral Kaye-BKZ model (Kaye, 1962 and Bernstein, Kearsley, and Zapas, 1963) predicts a shear-thinning behaviour of $-N_2/N_1$ decreasing from 0.11 at low shear rates to vanishing small at high shear rates. The predictions of the Doi Edwards model (Doi and Edwards, 1988) are sensitive to assumptions but gives a reasonable value of $-N_2/N_1=2/7$ in the low shear rate limit.

5. Summary and outlook

We have reviewed the many flows where second normal-stress differences "N_2" in complex fluids may give rise to important effects. Broadly, one can think about this property as affecting two wide classes of flow problems. Firstly, in straight ducts, even in the limit of vanishingly small inertia where Newtonian fluids remain unidirectional, gradients of N_2 may drive a secondary flow in any geometry outside of those with perfectly circular cross sections. Such secondary flows can significantly modify heat and mass transport over the equivalent unidirectional flow for example. They can even occur in pipe flows should the flow not be running "full" such that there is a free surface which imparts a gradient of N_2 to the flow. Secondly, more generally, flows in which there is a free surface or layers of fluids with different properties – such that there is a jump in N_2 across the interface – appear sensitive to instabilities the driving mechanism for which is due to N_2. As most "standard" rheological measurements

incorporate flows with free surfaces, the importance of N_2 in limiting measurements at high rates, such as in "edge fracture", is clear. Presumably there are many other flows – such as die swell for example – where N_2 may be important for certain complex fluids or in certain circumstances. It is likely that other flow problems will arise where N_2 is discovered to be of importance.

Although, as we have documented in section 2, many different techniques have been proposed to experimentally determine N_2, routine measurements remain challenging and this would appear to us as a major unresolved problem before any such measurements can become as routine as viscosity or N_1. In particular, a number of techniques which require multiple measurements using different samples and/or differentiation of (necessarily imperfect) experimental data carry large uncertainty. Techniques where the fluid free surface itself acts as a pressure "gauge" – such as the semi-circular tilted trough experiment or the rod climbing/dipping experiment – are useful in being able to visually unequivocally demonstrate the sign of N_2 whilst also being able to determine quantitative values (with sufficient work). Unfortunately, the rod experiment also requires a separate measurement to determine N_1. The tilted trough experiment appears to offer potential but requires a bespoke experimental facility and rather large amounts of fluid (plus necessarily a rather complicated data processing technique to extract N_2). Thus, it would seem to us that the best approach – and most likely to gain widespread adoption – are the techniques which make use of flush-mounted pressure transducers in order to determine pressure gradients under cone-and-plate or parallel-plate flows. Such geometries are routinely used for measuring the shear viscosity of a wide range of complex fluids and the incorporation of such pressure transducers in commercial rheometers, in addition to the force-rebalance transducers which are routinely used to be able to determine the axial thrust, would represent a step change in this area.

Surveying the literature for measurements of N_2 for complex fluids is quite revealing. The two largest classes of fluids for which various data sets exists are polymeric solutions/melts and dense colloidal suspensions primarily in Newtonian base fluids (although there are a number of data sets where the matrix fluid itself is polymeric). The most developed literature is the polymeric where, outside of the dilute solution limit where N_2 does appear to be negligibly small, N_2 seems unequivocally to be negative in sign and up to 30% of N_1 especially at low shear rates. At these values it seems hard to classify N_2 as being negligible. Nevertheless, there is some limited data for aqueous solutions (or water/glycerol solvents) of commercial grade polyethylene oxide and polyacrylamides which show $N_2 \sim 0.05\text{-}0.1\ N_1$ where such a

categorisation would seem more reasonable. Studies using the cone-and-plate pressure-gradient method for such polymers whilst systematically varying molecular weight, concentration and solvent viscosity/quality etc would be welcome.

Before leaving our discussion of polymeric fluids, we note that all of the polymer solutions discussed in this review are for "flexible" systems and N_2 data for semi-rigid polymeric solutions, such as xanthan gum, would also be welcome. Although measurements of normal-stresses for such fluids in aqueous solution – which are often incorrectly classified as "inelastic" – are notably challenging, recent progress has been made with parallel plate geometries and very small gaps to probe high shear rates (Dakhil, Auhl, and Wierschem, 2019).

The N_2 data sets for the second most studied system – namely dense non-Brownian suspensions – have reinvigorated the techniques to measure N_2 that were originally proposed for polymeric systems. In so doing, it has been found that N_2 is the significant normal-stress difference and larger than N_1, and these studies have shown the importance, and value, of not simply neglecting this property based on results for other complex fluid systems where it is indeed negligible. As we mentioned in the introduction, there are many other complex fluids, for example emulsions, foams, surfactant solutions in different phases outside of semi-dilute wormlike where nematic and/or hexagonal phases can be formed, where a knowledge of the second-normal stress difference is limited or non-existent, which could equally benefit from measurements of this property. Recent interesting normal-stress data for emulsion and foam systems was made via thrust measurements in a parallel plate geometry and reported simply as N_1-N_2 (Habibi, Dinkgreve, Paredes, et al., 2016) i.e. no attempt is made to separate out the relative contributions. Interestingly, although fluids exhibiting $N_1 \sim -N_2$ don't seem to have been reported in the experimental literature, such behaviour has been predicted to occur theoretically for fluids, such as foams or dense emulsions, exhibiting "sheet-like" or "film-fluid-like" behaviour (Larson, 1997). In this paper, Larson, 1997 shows that for certain film models the predicted behaviour is precisely $N_1 = -N_2$ and offers the following explanation "Films, on the other hand, orient parallel to the XZ plane in shear so that both τ_{xx} and τ_{zz} are large compared to τ_{yy}. This implies that $N_2 \sim -N_1$ for films." Larson, 1997 goes on to state that "Measurements of N_2 for foams, emulsions, and blends would, therefore, be of considerable interest. None, however, have been reported as yet". We note, 20 years after this statement, our review of the literature indicates that this is still the case. Connecting this back to the Oldroyd-A model which we highlighted in our final section as being the simplest differential model to include N_2 effects, Larson, 2019, notes that "microscopically, the Oldroyd-B model deals with affinely

stretching filaments (or polymers) that one might call "line fluids," while Oldroyd-A describes affinely stretching planes or "film fluids." Thus, Oldroyd-A should be more appropriate for foams, dense emulsions, and other fluids containing sheet-like stretchable elastic objects." Although it has long been neglected as being "unphysical", we note that for some fluids the Oldroyd-A model may represent a reasonable "first approximation" to probe effects due to second normal-stress differences in a flow. Much as the Oldroyd-B benefits from a constant shear viscosity – allowing effects of N_1 to be probed without the "complication" of shear-thinning (and effects to be "separated out") – the Oldroyd-A could offer a similar toy model but with strong N_2 effects, that is potentially analytically tractable, but not restricted to a certain class of motions (such as the second order fluid). Comparison of the N_2 response for the other models commonly used, namely the Johnson-Segalman, Phan-Thien and Tanner and Giesekus models, highlights a number of interesting points. Firstly, these models are all nearly 40 years old – all appearing within a 5-year period beginning at the end of the 70s – and more recent microscopically-informed models all predict vanishing N_2 in steady simple shear. Secondly, N_2 in steady simple shear flow can be incorporated into simple differential models in two key ways: either by an inclusion of an lower-convected derivative component as in the Oldroyd-A, co-rotational Oldroyd, JS and PTT models, or by a quadratic stress term as in the Giesekus. At low shear rates these models all exhibit very similar behaviour with both normal-stress differences growing quadratically in shear rate and N_2 being negative and proportional to N_1 through the non-linear parameter. The response at higher rates is more interesting and the JS/PTT model predictions diverge from the Giesekus. As Larson noted (Larson, 1988), N_2 appears to offer a sensitive test of constitutive equations and data for more systems in this high shear rate limit is crucially required here.

Acknowledgements - RJP acknowledges funding for a Fellowship in Complex Fluids & Rheology from the Engineering and Physical Sciences Research Council (EPSRC) under grant number (EP/M025187/1). We are grateful for insightful discussions with Professor Anke Lindner (ESPCI, Paris) and Dr. Mahdi Davoodi (Schlumberger Cambridge Research). Helpful comments from the referees are also acknowledged.

References

Alves, M. A., Oliveira, P. J., Pinho, F. T. (2003). Benchmark solutions for the flow of Oldroyd-B and PTT fluids in planar contractions. *Journal of Non-Newtonian Fluid Mechanics*, *110*(1), 45–75. https://doi.org/10.1016/S0377-0257(02)00191-X

Alves, M. A., Pinho, F. T., Oliveira, P. J. (2001). Study of steady pipe and channel flows of a single-mode Phan-Thien-Tanner fluid. *Journal of Non-Newtonian Fluid Mechanics*, *101*(1–3), 55–76. https://doi.org/10.1016/S0377-0257(01)00159-8

Aral, B. K., Kalyon, D. M. (1997). Viscoelastic material functions of noncolloidal suspensions with spherical particles. *Journal of Rheology*, *41*(3), 599–620. https://doi.org/10.1122/1.550841

Avagliano, A., Phan-Thien, N. (1998). Torsional flow: Effect of second normal stress difference on elastic instability in a finite domain. *Journal of Fluid Mechanics*, *359*, 217–237. https://doi.org/10.1017/S0022112097008434

Baek, S. G., Magda, J. J. (2003). Monolithic rheometer plate fabricated using silicon micromachining technology and containing miniature pressure sensors for N1 and N2 measurements. *Journal of Rheology*, *47*(5), 1249–1260. https://doi.org/10.1122/1.1595095

Baek, S. G., Magda, J. J., Larson, R. G. (1993). Rheological differences among liquid-crystalline polymers. I. The first and second normal stress differences of PBG solutions. *Journal of Rheology*, *37*(6), 1201–1224. https://doi.org/10.1122/1.550377

Baird, D. G. (1975). A Possible Method for Determining Normal Stress Differences from Hole Pressure Error Data. *Transactions of the Society of Rheology*, *19*(1), 147–151. https://doi.org/10.1122/1.549392

Baltussen, M. G. H. M., Verbeeten, W. M. H., Bogaerds, A. C. B., Hulsen, M. A., Peters, G. W. M. (2010). Anisotropy parameter restrictions for the eXtended Pom-Pom model. *Journal of Non-Newtonian Fluid Mechanics*, *165*(19–20), 1047–1054. https://doi.org/10.1016/j.jnnfm.2010.05.002

Barnes, H. A., Hutton, J. F., Walters, K. (1989). *An Introduction to Rheology* (Vol. 1). (New York): Elsevier Science.

Beavers, G. S., Joseph, D. D. (1975). The rotating rod viscometer. *Journal of Fluid Mechanics*, *69*(3), 475–511. https://doi.org/10.1017/S002211207500153X

Beris, A. N., Avgousti, M., Souvaliotis, A. (1992). Spectral calculations of viscoelastic flows: evaluation of the Giesekus constitutive equation in model flow problems. *Journal of Non-Newtonian Fluid Mechanics*, *44*(C), 197–228. https://doi.org/10.1016/0377-0257(92)80051-X

Bernstein, B., Kearsley, E. A., Zapas, L. J. (1963). A Study of Stress Relaxation with Finite Strain. *Transactions of the Society of Rheology*, *7*(1), 391–410. https://doi.org/10.1122/1.548963

Bird, R. B., Armstrong, R. C., Hassager, O. (1987). Dynamics of polymeric liquids. Vol. 1, 2nd Ed. : Fluid mechanics, *1*(18088690).

Boger, D. V. (1977). A highly elastic constant-viscosity fluid. *Journal of Non-Newtonian Fluid Mechanics*, *3*(1), 87–91. https://doi.org/10.1016/0377-0257(77)80014-1

Boyer, F., Pouliquen, O., Guazzelli, É. (2011). Dense suspensions in rotating-rod flows: Normal stresses and particle migration. *Journal of Fluid Mechanics*, *686*, 5–25. https://doi.org/10.1017/jfm.2011.272

Brady, J. F., Carpen, I. C. (2002). Second normal stress jump instability in non-Newtonian fluids. *Journal of Non-Newtonian Fluid Mechanics*, *102*(2), 219–232. https://doi.org/10.1016/S0377-0257(01)00179-3

Broadbent, J. M., Kaye, A., Lodge, A. S., Vale, D. G. (1968). Possible systematic error in the measurement of normal stress differences in polymer solutions in steady Shear Flow. *Nature*, *217*(5123), 55–56. https://doi.org/10.1038/217055a0

Brown, E. F., Burghardt, W. R., Kahvand, H., Venerus, D. C. (1995). Comparison of optical and mechanical measurements of second normal stress difference relaxation following step strain. *Rheologica Acta*, *34*(3), 221–234. https://doi.org/10.1007/BF00396013

Casanellas, L., Alves, M. A., Poole, R. J., Lerouge, S., Lindner, A. (2016). The stabilizing effect of shear thinning on the onset of purely elastic instabilities in serpentine microflows. *Soft Matter*, *12*(29), 6167–6175. https://doi.org/10.1039/c6sm00326e

Christiansen, E. B., Leppard, W. R. (1974). Steady-State and Oscillatory Flow Properties of Polymer Solutions. *Trans Soc Rheol*, *18*(1), 65–86. https://doi.org/10.1122/1.549327

Costanzo, S., Huang, Q., Ianniruberto, G., Marrucci, G., Hassager, O., Vlassopoulos, D. (2016). Shear and Extensional Rheology of Polystyrene Melts and Solutions with the Same Number of Entanglements. *Macromolecules*, *49*(10), 3925–3935. https://doi.org/10.1021/acs.macromol.6b00409

Costanzo, S., Ianniruberto, G., Marrucci, G., Vlassopoulos, D. (2018). Measuring and assessing first and second normal stress differences of polymeric fluids with a modular cone-partitioned plate geometry. *Rheologica Acta*, *57*(5), 363–376. https://doi.org/10.1007/s00397-018-1080-1

Couturier, É., Boyer, F., Pouliquen, O., Guazzelli, É. (2011). Suspensions in a tilted trough: Second normal stress difference. *Journal of Fluid Mechanics*, *686*, 26–39. https://doi.org/10.1017/jfm.2011.315

Cwalina, C. D., Wagner, N. J. (2014). Material properties of the shear-thickened state in concentrated near hard-sphere colloidal dispersions. *Journal of Rheology*, *58*(4), 949–967. https://doi.org/10.1122/1.4876935

Dai, S., Bertevas, E., Qi, F., Tanner, R. I. (2013). Viscometric functions for noncolloidal sphere suspensions with Newtonian matrices. *Journal of Rheology*, *57*(2), 493–510. https://doi.org/10.1122/1.4774325

Dai, S., Qi, F., Tanner, R. I. (2014). Viscometric functions of concentrated non-colloidal suspensions of spheres in a viscoelastic matrix. *Journal of Rheology*, *58*(1), 183–198. https://doi.org/10.1122/1.4851336

Dakhil, H., Auhl, D., Wierschem, A. (2019). Infinite-shear viscosity plateau of salt-free aqueous xanthan solutions. *Journal of Rheology*, *63*(1), 63–69. https://doi.org/10.1122/1.5044732

Davies, G. A., Stokes, J. R. (2005). On the gap error in parallel plate rheometry that arises from the presence of air when zeroing the gap. *Journal of Rheology*, *49*(4), 919–922. https://doi.org/10.1122/1.1942501

Davoodi, M., Lerouge, S., Norouzi, M., Poole, R. J. (2018). Secondary flows due to finite aspect ratio in inertialess viscoelastic Taylor-Couette flow. *Journal of Fluid Mechanics*, *857*, 823–850. https://doi.org/10.1017/jfm.2018.746

Dbouk, T., Lobry, L., Lemaire, E. (2013). Normal stresses in concentrated non-Brownian suspensions. *Journal of Fluid Mechanics*, *715*, 239–272. https://doi.org/10.1017/jfm.2012.516

Debbaut, B., Avalosse, T., Dooley, J., Hughes, K. (1997). On the development of secondary motions in straight channels induced by the second normal stress difference: Experiments and simulations. *Journal of Non-Newtonian Fluid Mechanics*, *69*(2–3), 255–271. https://doi.org/10.1016/S0377-0257(96)01543-1

Denn, M. M., Morris, J. F. (2014). Rheology of Non-Brownian Suspensions. *Annu. Rev. Chem. Biomol. Eng*, *5*, 203–228. https://doi.org/10.1146/annurev-chembioeng-060713-040221

Doi, M., Edwards, S. F. (1988). *The Theory of Polymer Dynamics*. (Vol. 73), Clarendon Press-Oxford.

Fan, Y., Tanner, R. I., Phan-Thien, N. (2001). Fully developed viscous and viscoelastic flows in curved pipes. *Journal of Fluid Mechanics*, *440*, 327–357. https://doi.org/10.1017/S0022112001004785

Feng, H., Magda, J. J., Gale, B. K. (2019). Viscoelastic second normal stress difference dominated multiple-stream particle focusing in microfluidic channels. *Applied Physics Letters*, *115*(26), 263702. https://doi.org/10.1063/1.5129281

Frattini, P. L., Fuller, G. G. (1984). Note: A Note on Phase-Modulated Flow Birefringence: A Promising Rheo-Optical Method. *Journal of Rheology*, *28*(1), 61–70. https://doi.org/10.1122/1.549768

Fröhlich, H., Sack, R. (1946). Theory of the rheological properties of dispersions. *Proceedings of the Royal Society of London. Series A, Mathematical and Physical Sciences*, *185*(1003), 415–430. https://doi.org/10.1098/rspa.1946.0028

Gamonpilas, C., Morris, J. F., Denn, M. M. (2016). Shear and normal stress measurements in non-Brownian monodisperse and bidisperse suspensions. *Journal of Rheology*, *60*(2), 289–296. https://doi.org/10.1122/1.4942230

Gamonpilas, C., Morris, J. F., Denn, M. M. (2018). Erratum: “Shear and normal stress measurements in non-Brownian monodisperse and bidisperse suspensions” [J. Rheol. 60 (2), 289–296 (2016)]. *Journal of Rheology*, *62*(2), 665–667. https://doi.org/10.1122/1.5003086

Gao, H. W., Ramachandran, S., Christiansen, E. B. (1981). Dependency of the Steady-State and Transient Viscosity and First and Second Normal Stress Difference Functions on Molecular Weight for Linear Mono and Polydisperse Polystyrene Solutions. *Journal of Rheology*, *25*(2), 213–235. https://doi.org/10.1122/1.549617

Gao, S. X., Hartnett, J. P. (1996). Heat transfer behavior of Reiner-Rivlin fluids in rectangular ducts. *International Journal of Heat and Mass Transfer*, *39*(6), 1317–1324. https://doi.org/10.1016/0017-9310(95)00041-0

Gervang, B., Larsen, P. S. (1991). Secondary flows in straight ducts of rectangular cross section. *Journal of Non-Newtonian Fluid Mechanics*, *39*(3), 217–237.

https://doi.org/10.1016/0377-0257(91)80016-D

Giacomin, A. J., Bird, R. B., Johnson, L. M., Mix, A. W. (2011). Large-amplitude oscillatory shear flow from the corotational Maxwell model. *Journal of Non-Newtonian Fluid Mechanics*, *166*(19–20), 1081–1099. https://doi.org/10.1016/j.jnnfm.2011.04.002

Giesekus, H. (1982). A simple constitutive equation for polymer fluids based on the concept of deformation-dependent tensorial mobility. *Journal of Non-Newtonian Fluid Mechanics*, *11*(1–2), 69–109. https://doi.org/10.1016/0377-0257(82)85016-7

Ginn, R. F., Metzner, A. B. (1969). Measurement of Stresses Developed in Steady Laminar Shearing Flows of Viscoelastic Media. *Trans Soc Rheol*, *13*(4), 429–453. https://doi.org/10.1122/1.549138

Głowińska, E., Parcheta, P., Datta, J. (2019). Rheology of liquid crystalline polymers. In *Rheology of Polymer Blends and Nanocomposites: Theory, Modelling and Applications* (pp. 205–224). Elsevier. https://doi.org/10.1016/B978-0-12-816957-5.00010-0

Goddard, J. D., Miller, C. (1966). An inverse for the Jaumann derivative and some applications to the rheology of viscoelastic fluids. *Rheologica Acta*, *5*(3), 177–184. https://doi.org/10.1007/BF01982423

Graessley, W. W. (1980). Polymer chain dimensions and the dependence of viscoelastic properties on concentration, molecular weight and solvent power. *Polymer*, *21*(3), 258–262. https://doi.org/10.1016/0032-3861(80)90266-9

Graham, R. S., Likhtman, A. E., McLeish, T. C. B., Milner, S. T. (2003). Microscopic theory of linear, entangled polymer chains under rapid deformation including chain stretch and convective constraint release. *Journal of Rheology*, *47*(5), 1171–1200. https://doi.org/10.1122/1.1595099

Green, A. E., Rivlin, R. S. (1956). Steady flow of non-Newtonian fluids through tubes. *Quarterly of Applied Mathematics*, *14*(3), 299–308. https://doi.org/10.1090/qam/90335

Guazzelli, É., Pouliquen, O. (2018). Rheology of dense granular suspensions. *Journal of Fluid Mechanics*, *852*, P11–P173. https://doi.org/10.1017/jfm.2018.548

Guo, J., Meroney, R. N. (2013). Theoretical solution for laminar flow in partially-filled pipes. *Journal of Hydraulic Research*, *51*(4), 408–416. https://doi.org/10.1080/00221686.2013.784881

Habibi, M., Dinkgreve, M., Paredes, J., Bonn, D., Denn, M. M. (2016). Normal stress measurement in foams and emulsions in the presence of slip. *Journal of Non-Newtonian Fluid Mechanics*, *238*, 33–43. https://doi.org/10.1016/j.jnnfm.2016.06.008

Haleem, B. A., Nott, P. R. (2009). Rheology of particle-loaded semi-dilute polymer solutions. *Journal of Rheology*, *53*(2), 383–400. https://doi.org/10.1122/1.3073753

Harris, J. (1968). Measurement of normal stress differences in solutions of macromolecules. *Nature*, *217*(5135), 1248–1249. https://doi.org/10.1038/2171248a0

Hemingway, E. J., Fielding, S. M. (2019). Edge fracture instability in sheared complex fluids: Onset criterion and possible mitigation strategy. *Journal of Rheology*, *63*(5), 735–750. https://doi.org/10.1122/1.5095717

Hemingway, E. J., Kusumaatmaja, H., Fielding, S. M. (2017). Edge Fracture in Complex Fluids. *Physical Review Letters*, *119*(2), 028006.

https://doi.org/10.1103/PhysRevLett.119.028006

Hinch, E. J. (2011). The measurement of suspension rheology. *Journal of Fluid Mechanics*, *686*, 1–4. https://doi.org/10.1017/jfm.2011.350

Hinch, E. J. (2020). The much-neglected 2nd normal stress difference - YouTube. Retrieved October 25, 2020, from https://www.youtube.com/watch?v=VkVJO0QZhM8

Holroyd, G. A. J., Martin, S. J., Graham, R. S. (2017). Analytic solutions of the Rolie Poly model in time-dependent shear. *Journal of Rheology*, *61*(5), 859–870. https://doi.org/10.1122/1.4990639

Hongladarom, K., Burghardt, W. R. (1993). Molecular Alignment of Polymer Liquid Crystals in Shear Flows. 2. Transient Flow Behavior in Poly(benzyl glutamate) Solutions. *Macromolecules*, *26*(4), 785–794. https://doi.org/10.1021/ma00056a033

Hu, H. H., Riccius, O., Chen, K. P., Arney, M., Joseph, D. D. (1990). Climbing constant, second-order correction of Trouton's viscosity, wave speed and delayed die swell for M1. *Journal of Non-Newtonian Fluid Mechanics*, *35*(2–3), 287–307. https://doi.org/10.1016/0377-0257(90)85055-4

Huilgol, R. R., Panizza, M., Payne, L. E. (1993). On the rectilinear flow of a second-order fluid and the role of the second normal stress difference in edge fracture in rheometry. *Journal of Non-Newtonian Fluid Mechanics*, *50*(2–3), 331–348. https://doi.org/10.1016/0377-0257(93)80037-C

Hutton, J. F. (1963). Fracture of liquids in shear. *Nature*, *200*(4907), 646–648. https://doi.org/10.1038/200646a0

Hutton, J. F. (1972). Effect of changes of surface tension and contact angle on normal force measurement with the Weissenberg rheogoniometer. *Rheologica Acta*, *11*(1), 70–72. https://doi.org/10.1007/BF01992872

Inkson, N. J., Phillips, T. N. (2007). Unphysical phenomena associated with the extended pom-pom model in steady flow. *Journal of Non-Newtonian Fluid Mechanics*, *145*(2–3), 92–101. https://doi.org/10.1016/j.jnnfm.2007.05.002

Inn, Y. W., Wissbrun, K. F., Denn, M. M. (2005). Effect of edge fracture on constant torque rheometry of entangled polymer solutions. *Macromolecules*, *38*(22), 9385–9388. https://doi.org/10.1021/ma0510901

Isaki, T., Takahashi, M. (2002). Normal stress ratio predicted by viscoelastic constitutive equations. *Nihon Reoroji Gakkaishi*, *30*(1), 65–69. https://doi.org/10.1678/rheology.30.65

Jackson, R., Kaye, A. (1966). The measurement of the normal stress differences in a liquid undergoing simple shear flow using a cone-and-plate total thrust apparatus only. *British Journal of Applied Physics*, *17*(10), 1355–1360. https://doi.org/10.1088/0508-3443/17/10/314

James, D. F. (2009). Boger fluids. *Annual Review of Fluid Mechanics*, *41*, 129–142. https://doi.org/10.1146/annurev.fluid.010908.165125

Jensen, E. A., Christiansen, J. de C. (2008). Measurements of first and second normal stress differences in a polymer melt. *Journal of Non-Newtonian Fluid Mechanics*, *148*(1–3), 41–46. https://doi.org/10.1016/j.jnnfm.2007.04.011

Johnson, M. W., Segalman, D. (1977). A model for viscoelastic fluid behavior which allows non-affine deformation. *Journal of Non-Newtonian Fluid Mechanics*, *2*(3), 255–270. https://doi.org/10.1016/0377-0257(77)80003-7

Joseph, D. D., Beavers, G. S. (1977). Free surface problems in rheological fluid mechanics. *Rheologica Acta*, *16*(2), 169–189. https://doi.org/10.1007/BF01527914

Kalogrianitis, S. G., van Egmond, J. W. (1997). Full tensor optical rheometry of polymer fluids. *Journal of Rheology*, *41*(2), 343–364. https://doi.org/10.1122/1.550806

Kaye, A. (1962). Non-Newtonian Flow in Incompressible Fluids. *College of Aeronautics, Cranfield, UK*, *Note 134*.

Kearsley, E. A. (1970). Intrinsic Errors for Pressure Measurements in a Slot along a Flow. *Trans Soc Rheol*, *14*(3), 419–424. https://doi.org/10.1122/1.549171

Keentok, M., Georgescu, A. G., Sherwood, A. A., Tanner, R. I. (1980). The measurement of the second normal stress difference for some polymer solutions. *Journal of Non-Newtonian Fluid Mechanics*, *6*(3–4), 303–324. https://doi.org/10.1016/0377-0257(80)80008-5

Keentok, M., Tanner, R. I. (1982). Cone-Plate and Parallel Plate Rheometry of Some Polymer Solutions. *Journal of Rheology*, *26*(3), 301–311. https://doi.org/10.1122/1.549684

Keentok, M., Xue, S. C. (1999). Edge fracture in cone-plate and parallel plate flows. *Rheologica Acta*, *38*(4), 321–348. https://doi.org/10.1007/s003970050184

Kim, S., Mewis, J., Clasen, C., Vermant, J. (2013). Superposition rheometry of a wormlike micellar fluid. *Rheologica Acta*, *52*(8–9), 727–740. https://doi.org/10.1007/s00397-013-0718-2

Kotaka, T., Michio, K., Mikio, T. (1959). Normal Stress Effect in Concentrated Polymer Solutions. *Trans Soc Rheol*, *42*(2), 641–643. https://doi.org/10.1143/JPSJ.42.641

Kulicke, W. M., Wallbaum, U. (1985). Determination of first and second normal stress differences in polymer solutions in steady shear flow and limitations caused by flow irregularities. *Chemical Engineering Science*, *40*(6), 961–972. https://doi.org/10.1016/0009-2509(85)85009-0

Larson, R. G. (1988). *Constitutive Equations for Polymer Melts and Solutions*. *Constitutive Equations for Polymer Melts and Solutions*. Elsevier. https://doi.org/10.1016/c2013-0-04284-3

Larson, R. G. (1997). The elastic stress in "film fluids." *Journal of Rheology*, *41*(2), 365–372. https://doi.org/10.1122/1.550857

Larson, R. G. (2019). *Private Communication*.

Laun, H. M. (1994). Normal stresses in extremely shear thickening polymer dispersions. *Journal of Non-Newtonian Fluid Mechanics*, *54*(C), 87–108. https://doi.org/10.1016/0377-0257(94)80016-2

Laun, H. M., Gabriel, C., Schmidt, G. (2008). Primary and secondary normal stress differences of a magnetorheological fluid (MRF) up to magnetic flux densities of 1 T. *Journal of Non-Newtonian Fluid Mechanics*, *148*(1–3), 47–56. https://doi.org/10.1016/j.jnnfm.2007.04.019

Lee, C. S., Magda, J. J., DeVries, K. L., Mays, J. W. (1992). Measurements of the Second Normal Stress Difference for Star Polymers with Highly Entangled Branches. *Macromolecules*, *25*(18), 4744–4750. https://doi.org/10.1021/ma00044a041

Lee, C. S., Tripp, B. C., Magda, J. J. (1992). Does N1 or N2 control the onset of edge fracture? *Rheologica Acta*, *31*(3), 306–308. https://doi.org/10.1007/BF00366509

Lee, J.-Y., Magda, J. J., Hu, H., Larson, R. G. (2002). Cone angle effects, radial pressure profile, and second normal stress difference for shear-thickening wormlike micelles. *Journal of Rheology*, *46*(1), 195–208. https://doi.org/10.1122/1.1428319

Leonov, A. I. (1976). Nonequilibrium thermodynamics and rheology of viscoelastic polymer media. *Rheologica Acta*, *15*(2), 85–98. https://doi.org/10.1007/BF01517499

Lerouge, S., Olmsted, P. D. (2020). Non-local Effects in Shear Banding of Polymeric Flows. *Frontiers in Physics*, *7*, 246. https://doi.org/10.3389/fphy.2019.00246

Letelier, M. F., Acosta, M., Córdova, J., Siginer, D. A. (2002). Steady secondary flows of Phan-Thien-Tanner fluids in the vicinity of a corner. In *ASME International Mechanical Engineering Congress and Exposition, Proceedings* (pp. 291–295). American Society of Mechanical Engineers (ASME). https://doi.org/10.1115/IMECE2002-32233

Letelier, M. F., Siginer, D. A., Almendra, D. L., Stockle, J. (2019). Secondary flows in eccentric-annular tubes. In *ASME International Mechanical Engineering Congress and Exposition, Proceedings (IMECE)* (Vol. 7). American Society of Mechanical Engineers (ASME). https://doi.org/10.1115/IMECE2019-11548

Likhtman, A. E., Graham, R. S. (2003). Simple constitutive equation for linear polymer melts derived from molecular theory: Rolie-Poly equation. *Journal of Non-Newtonian Fluid Mechanics*, *114*(1), 1–12. https://doi.org/10.1016/S0377-0257(03)00114-9

Lin, Y., Phan-Thien, N., Cheong Khoo, B. (2014). Normal stress differences behavior of polymeric particle suspension in shear flow. *Journal of Rheology*, *58*(1), 223–235. https://doi.org/10.1122/1.4855496

López-López, M. T., Kuzhir, P., Durán, J. D. G., Bossis, G. (2010). Normal stresses in a shear flow of magnetorheological suspensions: Viscoelastic versus Maxwell stresses. *Journal of Rheology*, *54*(5), 1119–1136. https://doi.org/10.1122/1.3479043

Magda, J. J., Baek, S. G. (1994). Concentrated entangled and semidilute entangled polystyrene solutions and the second normal stress difference. *Polymer*, *35*(6), 1187–1194. https://doi.org/10.1016/0032-3861(94)90010-8

Magda, J. J., Baek, S. G., DeVries, K. L., Larson, R. G. (1991). Shear Flows of Liquid Crystal Polymers: Measurements of the Second Normal Stress Difference and the Doi Molecular Theory. *Macromolecules*, *24*(15), 4460–4468. https://doi.org/10.1021/ma00015a034

Magda, J. J., Lou, J., Baek, S. G., DeVries, K. L. (1991). Second normal stress difference of a Boger fluid. *Polymer*, *32*(11), 2000–2009. https://doi.org/10.1016/0032-3861(91)90165-F

Malkus, D. S., Pritchard, W. G., Yao, M. (1992). The hole-pressure effect and viscometry. *Rheologica Acta*, *31*(6), 521–534. https://doi.org/10.1007/BF00367007

Mall-Gleissle, S. E., Gleissle, W., McKinley, G. H., Buggisch, H. (2002). The normal stress behaviour of suspensions with viscoelastic matrix fluids. *Rheologica Acta*, *41*(1), 61–76.

https://doi.org/10.1007/s003970200006

Marsh, B. D., Pearson, J. R. A. (1968). The measurement of normal-stress differences using a cone- and-plate total thrust apparatus. *Rheologica Acta*, *7*(4), 326–331. https://doi.org/10.1007/BF01984846

McKinley, G. H., Pakdel, P., Öztekin, A. (1996). Rheological and geometric scaling of purely elastic flow instabilities. *Journal of Non-Newtonian Fluid Mechanics*, *67*(1–3), 19–47. https://doi.org/10.1016/S0377-0257(96)01453-X

McLeish, T. C. B., Larson, R. G. (1998). Molecular constitutive equations for a class of branched polymers: The pom-pom polymer. *Journal of Rheology*, *42*(1), 81–110. https://doi.org/10.1122/1.550933

Meissner, J., Garbella, R. W., Hostettler, J. (1989). Measuring Normal Stress Differences in Polymer Melt Shear Flow. *Journal of Rheology*, *33*(6), 843–864. https://doi.org/10.1122/1.550067

Mollica, F., Rajagopal, K. R. (1999). Secondary flows due to axial shearing of a third grade fluid between two eccentrically placed cylinders. *International Journal of Engineering Science*, *37*(4), 411–429. https://doi.org/10.1016/s0020-7225(98)00057-3

Moorcroft, R. L., Fielding, S. M. (2014). Shear banding in time-dependent flows of polymers and wormlike micelles. *Journal of Rheology*, *58*(1), 103–147. https://doi.org/10.1122/1.4842155

Morozov, A., Spagnolie, S. E. (2015). Introduction to Complex Fluids (pp. 3–52). Springer, New York, NY. https://doi.org/10.1007/978-1-4939-2065-5_1

Morrison, F. A. (2001). *Understanding Rheology*. Oxford University Press. Retrieved from https://books.google.co.uk/books?id=bwTn8ZbR0C4C

Ng, H. C. H., Cregan, H. L. F., Dodds, J. M., Poole, R. J., Dennis, D. J. C. (2018). Partially filled pipes: Experiments in laminar and turbulent flow. *Journal of Fluid Mechanics*, *848*, 467–507. https://doi.org/10.1017/jfm.2018.345

Ohl, N., Gleissle, W. (1992). The second normal stress difference for pure and highly filled viscoelastic fluids. *Rheologica Acta*, *31*(3), 294–305. https://doi.org/10.1007/BF00366508

Oldroyd, J. G. (1950). On the formulation of rheological equations of state. *Proceedings of the Royal Society of London. Series A. Mathematical and Physical Sciences*, *200*(1063), 523–541. https://doi.org/10.1098/rspa.1950.0035

Oldroyd, J. G. (1958). Non-Newtonian effects in steady motion of some idealized elastico-viscous liquids. *Proceedings of the Royal Society of London. Series A. Mathematical and Physical Sciences*, *245*(1241), 278–297. https://doi.org/10.1098/rspa.1958.0083

Olson, D. J., Brown, E. F., Burghardt, W. R. (1998). Second normal stress difference relaxation in a linear polymer melt following step-strain. *Journal of Polymer Science, Part B: Polymer Physics*, *36*(14), 2671–2675. https://doi.org/10.1002/(SICI)1099-0488(199810)36:14<2671::AID-POLB20>3.0.CO;2-7

Phan-Thien, N. (1978). A Nonlinear Network Viscoelastic Model. *Journal of Rheology*, *22*(3), 259–283. https://doi.org/10.1122/1.549481

Phan-Thien, N., Tanner, R. I. (1977). A new constitutive equation derived from network

theory. *Journal of Non-Newtonian Fluid Mechanics*, *2*(4), 353–365. https://doi.org/10.1016/0377-0257(77)80021-9

Pipe, C. J., Kim, N. J., Vasquez, P. A., Cook, L. P., McKinley, G. H. (2010). Wormlike micellar solutions: II. Comparison between experimental data and scission model predictions. *Journal of Rheology*, *54*(4), 881–913. https://doi.org/10.1122/1.3439729

Pollett, W. F. O. (1955). Rheological behaviour of continuously sheared polythene. *British Journal of Applied Physics*, *6*(6), 199–206. https://doi.org/10.1088/0508-3443/6/6/304

Poole, R. J. (2016). Measuring normal-stresses in torsional rheometers : a practical guide. *The British Society of Rheology, Rheology Bulletin*, *57(2)*, 36–46.

Poungthong, P., Giacomin, A. J., Saengow, C., Kolitawong, C. (2019). Exact solution for intrinsic nonlinearity in oscillatory shear from the corotational Maxwell fluid. *Journal of Non-Newtonian Fluid Mechanics*, *265*, 53–65. https://doi.org/10.1016/j.jnnfm.2019.01.001

Ramachandran, A., Leighton, D. T. (2008). The influence of secondary flows induced by normal stress differences on the shear-induced migration of particles in concentrated suspensions. *Journal of Fluid Mechanics*, *603*, 207–243. https://doi.org/10.1017/S0022112008000980

Ramachandran, S., Gao, H. W., Christiansen, E. B. (1985). Dependence of Viscoelastic Flow Functions on Molecular Structure for Linear and Branched Polymers. *Macromolecules*, *18*(4), 695–699. https://doi.org/10.1021/ma00146a021

Rautenbach, R., Schümmer, P., Petersen, J. F. (1975). Zur Bestimmung der Normalspannungs-Funktionen von Hochpolymeren mittels der Kegel-Platte-Abstand-Anordnung (KPA). *Rheologica Acta*, *14*(11), 968–975. https://doi.org/10.1007/bf01516299

Rehage, H., Hoffmann, H. (1991). Viscoelastic surfactant solutions:Model systems for theological research. *Molecular Physics*, *74*(5), 933–973. https://doi.org/10.1080/00268979100102721

Renardy, Y. Y. (1988). Stability of the interface in two-layer couette flow of upper convected maxwell liquids. *Journal of Non-Newtonian Fluid Mechanics*, *28*(1), 99–115. https://doi.org/10.1016/0377-0257(88)80012-0

Renardy, Y. Y., Renardy, M. (1998). Instability due to second normal stress jump in two-layer shear flow of the Giesekus fluid. *Journal of Non-Newtonian Fluid Mechanics*, *81*(3), 215–234. https://doi.org/10.1016/S0377-0257(98)00125-6

Rothstein, J. P., Mohammadigoushki, H. (2020, November 1). Complex flows of viscoelastic wormlike micelle solutions. *Journal of Non-Newtonian Fluid Mechanics*. Elsevier B.V. https://doi.org/10.1016/j.jnnfm.2020.104382

Schweizer, T. (2002). Measurement of the first and second normal stress differences in a polystyrene melt with a cone and partitioned plate tool. *Rheologica Acta*, *41*(4), 337–344. https://doi.org/10.1007/s00397-002-0232-4

Schweizer, T., Hostettler, J., Mettler, F. (2008). A shear rheometer for measuring shear stress and both normal stress differences in polymer melts simultaneously: The MTR 25. *Rheologica Acta*, *47*(8), 943–957. https://doi.org/10.1007/s00397-008-0300-5

Schweizer, T., Schmidheiny, W. (2013). A cone-partitioned plate rheometer cell with three

partitions (CPP3) to determine shear stress and both normal stress differences for small quantities of polymeric fluids. *Journal of Rheology*, *57*(3), 841–856. https://doi.org/10.1122/1.4797458

Shaqfeh, E. S. (1996). Purely elastic instabilities in viscometric flows. *Annual Review of Fluid Mechanics*, *28*, 129–185. https://doi.org/10.1146/annurev.fl.28.010196.001021

Shaqfeh, E. S., Larson, R. G. (1992). The effects of gap width and dilute solution properties on the viscoelastic Taylor-Couette instability. *Journal of Fluid Mechanics*, *235*, 285–317. https://doi.org/10.1017/S0022112092001113

Sharma, V., McKinley, G. H. (2012). An intriguing empirical rule for computing the first normal stress difference from steady shear viscosity data for concentrated polymer solutions and melts. *Rheologica Acta*, *51*(6), 487–495. https://doi.org/10.1007/s00397-011-0612-8

Siginer, D. A. (2011). Isothermal tube flow of non-linear viscoelastic fluids. Part II: Transversal field. *International Journal of Engineering Science*, *49*(6), 443–465. https://doi.org/10.1016/j.ijengsci.2010.11.001

Siginer, D. A., Letelier, M. F. (2010). Heat transfer asymptote in laminar flow of non-linear viscoelastic fluids in straight non-circular tubes. *International Journal of Engineering Science*, *48*(11), 1544–1562. https://doi.org/10.1016/j.ijengsci.2010.07.010

Siginer, D. A., Letelier, M. F. (2011). Laminar flow of non-linear viscoelastic fluids in straight tubes of arbitrary contour. *International Journal of Heat and Mass Transfer*, *54*(9–10), 2188–2202. https://doi.org/10.1016/j.ijheatmasstransfer.2010.11.041

Singh, A., Nott, P. R. (2003). Experimental measurements of the normal stresses in sheared Stokesian suspensions. *Journal of Fluid Mechanics*, *490*(490), 293–320. https://doi.org/10.1017/S0022112003005366

Snijkers, F., Vlassopoulos, D. (2011). Cone-partitioned-plate geometry for the ARES rheometer with temperature control. *Journal of Rheology*, *55*(6), 1167–1186. https://doi.org/10.1122/1.3625559

Snook, B., Davidson, L. M., Butler, J. E., Pouliquen, O., Guazzelli, É. (2014). Normal stress differences in suspensions of rigid fibres. *Journal of Fluid Mechanics*, *758*, 486–507. https://doi.org/10.1017/jfm.2014.541

Speziale, C. G. (1984). On the development of non-Newtonian secondary flows in tubes of non-circular cross-section. *Acta Mechanica*, *51*(1–2), 85–95. https://doi.org/10.1007/BF01176390

Sui, C., McKenna, G. B. (2007). Instability of entangled polymers in cone and plate rheometry. *Rheologica Acta*, *46*(6), 877–888. https://doi.org/10.1007/s00397-007-0169-8

Tadmor, Z., Bird, R. B. (1974). Rheological analysis of stabilizing forces in wire-coating dies. *Polymer Engineering & Science*, *14*(2), 124–136. https://doi.org/10.1002/pen.760140208

Takahashi, T., Shirakashi, M., Miyamoto, K., Fuller, G. G. (2002). Development of a double-beam rheo-optical analyzer for full tensor measurement of optical anisotropy in complex fluid flow. *Rheologica Acta*, *41*(5), 448–455. https://doi.org/10.1007/s00397-002-0226-2

Tanner, R. I. (1970). Some Methods for Estimating the Normal Stress Functions in

Viscometric Flows. *Trans Soc Rheol*, *14*, 483. https://doi.org/10.1122/1.549175

Tanner, R. I. (1988). Pressure-hole errors-an alternative approach. *Journal of Non-Newtonian Fluid Mechanics*, *28*(3), 309–318. https://doi.org/10.1016/0377-0257(88)87003-4

Tanner, R. I. (2018, October 1). Review Article: Aspects of non-colloidal suspension rheology. *Physics of Fluids*. American Institute of Physics Inc. https://doi.org/10.1063/1.5047535

Tanner, R. I. (2019). Review: Rheology of noncolloidal suspensions with non-Newtonian matrices. *Journal of Rheology*, *63*(4), 705–717. https://doi.org/10.1122/1.5085363

Tanner, R. I., Dai, S. (2019). Edge fracture in non-colloidal suspensions. *Journal of Non-Newtonian Fluid Mechanics*, *272*, 104171. https://doi.org/10.1016/j.jnnfm.2019.104171

Tanner, R. I., Keentok, M. (1983). Shear Fracture in Cone-Plate Rheometry. *Journal of Rheology*, *27*(1), 47–57. https://doi.org/10.1122/1.549698

Tanner, R. I., Nasseri, S. (2003). Simple constitutive models for linear and branched polymers. *Journal of Non-Newtonian Fluid Mechanics*, *116*(1), 1–17. https://doi.org/10.1016/j.jnnfm.2003.08.001

Tanner, R. I., Pipkin, A. C. (1969). Intrinsic Errors in Pressure-Hole Measurements. *Trans Soc Rheol*, *13*(4), 471–484. https://doi.org/10.1122/1.549147

Townsend, P., Walters, K., Waterhouse, W. M. (1976). Secondary flows in pipes of square cross-section and the measurement of the second normal stress difference. *Journal of Non-Newtonian Fluid Mechanics*, *1*(2), 107–123. https://doi.org/10.1016/0377-0257(76)80011-0

van Es, H. E. (1974). A new method for determining the second normal stress difference in viscoelastic fluids. *Rheologica Acta*, *13*(6), 905–909. https://doi.org/10.1007/BF01526672

Verbeeten, W. M. H., Peters, G. W. M., Baaijens, F. P. T. (2001). Differential constitutive equations for polymer melts: The extended Pom–Pom model. *Journal of Rheology*, *45*(4), 823–843. https://doi.org/10.1122/1.1380426

Villone, M. M., D'Avino, G., Hulsen, M. A., Greco, F., Maffettone, P. L. (2013). Particle motion in square channel flow of a viscoelastic liquid: Migration vs. secondary flows. *Journal of Non-Newtonian Fluid Mechanics*, *195*, 1–8. https://doi.org/10.1016/j.jnnfm.2012.12.006

Weissenberg, K. (1947). A continuum theory of rheological phenomena. *Nature*, *159*(4035), 310. https://doi.org/10.1038/159310a0

Wheeler, E. K., Izu, P., Fuller, G. G. (1996). Structure and rheology of wormlike micelles. *Rheologica Acta*, *35*(2), 139–149. https://doi.org/10.1007/BF00396041

Whorlow, R. W. (1992). *Rheological techniques.* Simon & Schuster. Ellis Horwood series in physics and its applications. Retrieved from https://liverpool.idm.oclc.org/login?url=https://search.ebscohost.com/login.aspx?direct=true&db=cat00003a&AN=lvp.b1662929&site=eds-live&scope=site

Wilson, H. J., Rallison, J. M. (1997). Short wave instability of co-extruded elastic liquids with matched viscosities. *Journal of Non-Newtonian Fluid Mechanics*, *72*(2–3), 237–251. https://doi.org/10.1016/S0377-0257(97)00025-6

Wineman, A. S., Pipkin, A. C. (1966). Slow viscoelastic flow in tilted troughs. *Acta Mechanica*, *2*(1), 104–115. https://doi.org/10.1007/BF01176732

Wissbrun, K. F. (1981). Rheology of Rod-like Polymers in the Liquid Crystalline State. *Journal of Rheology*, *25*(6), 619–662. https://doi.org/10.1122/1.549634

Xue, S. C., Phan-Thien, N., Tanner, R. I. (1995). Numerical study of secondary flows of viscoelastic fluid in straight pipes by an implicit finite volume method. *Journal of Non-Newtonian Fluid Mechanics*, *59*(2–3), 191–213. https://doi.org/10.1016/0377-0257(95)01365-3

Yue, P., Dooley, J., Feng, J. J. (2008). A general criterion for viscoelastic secondary flow in pipes of noncircular cross section. *Journal of Rheology*, *52*(1), 315–332. https://doi.org/10.1122/1.2817674

Zarraga, I. E., Hill, D. A., Leighton, D. T. (2000). The characterization of the total stress of concentrated suspensions of noncolloidal spheres in Newtonian fluids. *Journal of Rheology*, *44*(2), 185–220. https://doi.org/10.1122/1.551083

Zarraga, I. E., Hill, D. A., Leighton, D. T. (2001). Normal stresses and free surface deformation in concentrated suspensions of noncolloidal spheres in a viscoelastic fluid. *Journal of Rheology*, *45*(5), 1065–1084. https://doi.org/10.1122/1.1396356

Zilz, J., Schäfer, C., Wagner, C., Poole, R. J., Alves, M. A., Lindner, A. (2014). Serpentine channels: Micro-rheometers for fluid relaxation times. *Lab on a Chip*, *14*(2), 351–358. https://doi.org/10.1039/c3lc50809a

Zrehen, A., Ramachandran, A. (2013). Demonstration of Secondary Currents in the Pressure-Driven Flow of a Concentrated Suspension Through a Square Conduit. *Physical Review Letters*, *110*(1), 018306. https://doi.org/10.1103/PhysRevLett.110.018306

Table 1: Summary of some second to first normal stress differences ratio for different fluid systems and the methods used to measure (N_1) and (N_2) along with the number of samples used in the measurements.

ID	Paper	Fluid Type	Fluid composition	Method	$(-N_2/N_1)$	No. of samples
1	Magda, Lou, et al., 1991	Boger Fluid	0.1 % of Polyisobutylene with molecular weight (M_W) = 1.3×10^6 in (polybutene + 2 chloropropane)	CP_G & RC	0.01 ± 0.01	2
		Polymer solution	NIST (polyisobutylene in cetan)	CP_G	0.15 ± 0.02	1
2	Hu et al., 1990	Boger Fluid	0.24 % of Polyisobutylene with M_W = 1.3×10^6 in oligomeric polybutene polybutene)	RC	0.11-0.12	2
3	Keentok et al., 1980	Boger Fluid	0.014% solution of Separan MGSOO in a mixture of maltose syrup and water	TT	~0	1
		Polymer solutions	1 and 0.7% solutions of a polyethylene oxide (Polyox WSR 301) in distilled water (a,b) 0.8,0.5 and 0.2% solutions of a polyacrylamide (Separan AP 30) in distilled water (c,d,e) 1.1% solution of Oppanol B 200 in decalin (f) "National Bureau of Standards Nonlinear Fluid No. 1".- 7.14% solution of polystyrene in a mixture of tricresyl phosphate and Arochlor (g)	TT	0.075 ± 0.01[a] 0.065 ± 0.01[b] 0.100 ± 0.01[c] 0.085 ± 0.015[d] 0.065 ± 0.01[e] 0.11 ± 0.01[f] 0.3 ± 0.10[g]	
4	Kalogrianitis and van Egmond, 1997	Polymer solution	6% of polystyrene with (M_W =$2x10^6$), M_W / M_n =1.06 in tricresyl phosphate, (semidilute, entangled regime)	Flow birefringence	0.1 to 0.2 increases to 0.9 at long times	1
5	H. W. Gao, Ramachandran, and Christiansen, 1981	Polymer solution	450 kg/m^3 mono and polydisperse polystyrene with (M_W =40-2000 kg/mol), M_W / M_n =1.06-22 in normal butylbenzene	CP_G & LAOS	0.22, 0.225 & 0.25	1
6	Christiansen and Leppard, 1974	Polymer solution	3% of polyethylene oxide in (57%-water, 38%-glycerine, and 5%-isopropyl-alcohol) and a 2.5% solution of polyacrylamide in (50%-water and 50%-glycerine)	CP_G & LAOS	0.07 & 0.09	1
7	Brown et al., 1995	Polymer solution	12wt% of high molecular weight, low polydispersity polystyrene with (M_W =$1.92x10^6$), M_W / M_n <1.3 dissolved in tricresylphosphate (TCP)	Flow birefringence & $CP\text{-}PP_T$	0.23 & 0.17	1,2
8	Magda and Baek, 1994	Polymer solution	22.9-255 kg/m^3 monodisperse polystyrene (PS) with M_W =581-4000 kg/mol, M_W / M_n =1-1.06 in n-butylbenzen , (semi-dilute and concentrated solutions)	CP_G	0.17 to 0.275 ± 0.005	1
9	Baek and Magda, 2003	Polymer solution	10 wt % of polyisobutylene in n-hexadecane (NIST SRM-1490)	CP_G	0.1 ± 0.02	1
10	Kulicke and Wallbaum, 1985	Polymer solutions	3-5 wt% polystyrene with (M_W =$1.86x10^6$ - $23.6x10^6$), M_W / M_n =1.1-1.3 in toluene, and 3 wt% polyacrylamide and polyacrylamide-co-sodium-acrylates in 0.1M Na,SO,/H,O solution	CPD_T	0.25-0.37	1
11	S. Ramachandran et al., 1985	Polymer solution (Linear)	450 kg/m^3 mono-and polydisperse linear polystyrenes with M_W =37-2000 kg/mol, M_W / M_n =1.06-22 in n-butylbenzen	CP_G	0.287 ± 2%	1
		Polymer solution (Star)	100-600 kg/m^3 four-arm-star poly-butadienes with M_w=300-330 kg/mol, M_W / M_n =1.78 in n-butylbenzen		0.214 ± 2%	1
12	Lee, Magda, et al., 1992	Polymer solution (Linear)	polyisoprenes with M_W =0.46 – $1x10^6$ and M_W / M_n =1.04 - 1.16	CP_G	0.17 & 0.2 ± 0.01	1
		Polymer solution (Star)	3-24% 6 and 10-arm polyisoperene with M_W =$0.59x10^6$-$0.64x10^6$), M_W / M_n =1.04 in tetradecane (TD)		0.21 & 0.3 ± 0.01	
13	Magda, Baek, et al., 1991	Liquid Crystals (Isotropic solution)	concentrated solutions of rodlike PBLG (poly(y-benzyl L-glutamate)) in m-creso (C < 9.5 wt%)	CP_G	0.29 ± 0.01	1

		Fully Liquid Crystalline Phase (LCP)	concentrated solutions of rodlike PBLG (poly(y-benzyl L-glutamate)) in m-creso (C >12.3 wt%)		>0.5 (N_2 is positive at some shear rates)	
14	Laun et al., 2008	Magnetorheological fluid (MRF)	50% of magnetizable spherical carbonyl iron powder particles (size several μm) in hydrocarbon oil.	CP-PP_T	~ - 0.25 (N_2 is Positive)	2
15	Costanzo et al., 2018	Polymer melt	(50 & 70%) of high-molar-mass Polystyrene PS (200 & 545 kg/mol) in a 2k oligostyrene (M_W = 2 kg/mol) at (130 & 170 °C)	CPP - Same sample, different stems	0.3 to 0.1	1
16	Olson et al., 1998	Polymer melt	highly monodisperse polyisoprene (M_W =130kg/mol), highly entangled with M_W / M_e =25 at room temperature	Flow birefringence	0.24 to 0.1	1
17	Schweizer, 2002	Polymer melt	polystyrene 158K (M_W =336 kg/mol), M_W / M_n =2.85 at 190 °C	CPP - Same stem, different samples	0.24 to 0.05	>2
18	Schweizer et al., 2008	Polymer melt	monodisperse polystyrene PS 206k (M_W =206 kg/mol), M_W / M_n =1.06 at 180 °C	CPP - Same sample, different stems	0.4 to 0.02	1
19	Schweizer and Schmidheiny, 2013	Polymer melt	PDMS 04A006 (Mw=2400kDa), M_W / M_n =2.5 at 30 °C	CPP3	0.24 to 0.1	1
20	Kim et al., 2013	Wormlike micellar solution	100 mM cetylpyridinium chloride, 60mM sodium salicylate, and 100mM NaCl	Superposition rheometry	0.21	2
21	J.-Y. Lee et al., 2002	Wormlike micellar solution	(5.0–10.0 mM) Equimolar solutions of CTAB and NaSS	CP_G	0.16 ± 0.005	1
22	Pipe et al., 2010	Wormlike micellar solution	100 mM/50 mM cetylpyridinium chloride (CPyCl, m0=340 g/mol) and sodium salicylate (NaSal, m0=160.1 g/mol) in 100 mM NaCl (upper end of the semi-dilute regime)	CP_G	0.4 to 0.1	1
23	Boyer et al., 2011	Newtonian Matrix Suspensions	20-50% polystyrene spherical beads with 140 and 230 μm average diameter in poly(ethylene glycol-ran-propylene glycol) monobutylether	RC	-	2
24	Couturier et al., 2011	Newtonian Matrix Suspensions	17-50% polystyrene spheres with 70 and 140 μm average diameter in poly(ethylene glycol-ran-propylene glycol) monobutylethe	TT	-1.6 to -5.8 (Both negative)	2
25	Cwalina and Wagner, 2014	Newtonian Matrix Suspensions	30-52% Silica nanoparticle with 520 nm average diameter in PEG, MW=200	CP-PP_T	-1.2 to -1.55 (Both negative)	2
26	Guazzelli and Pouliquen, 2018	Newtonian Matrix Suspensions	Review on different Newtonian matrix suspentions	Review on different methods	Review	*
27	Gamonpilas et al., 2016	Newtonian Matrix Suspensions	20-50% Mono- and bidisperse poly (methyl methacrylate) (PMMA) spheres with 10.1, 19.6, and 52.6 μm average diameter in 77.93% Triton X-100, 9.01% anhydrous zinc chloride, and 13.06% water (by weight)	CPD_T & PP_T	-1 to -2 (Both negative)	2
28	Laun, 1994	Newtonian Matrix Suspensions	58.7 vol.% of styrenelethyl acrylate copolymer particles with 280 nm average diameter in glycol	CP_T & CPP	0.5 (Assumed) N2 positive and N1 negative	2
29	Singh and Nott, 2003	Newtonian Matrix Suspensions	30-45% poly (methylmethacrylate) spheres with mean diameters of 116, 140 and 196 μm in 71.12 weight % Triton X-100, 12.40% water and 16.48% anhydrous zinc chloride.	Lock-in measurements in cylindrical-Couette and PP_G	-1 to -3.88 (Both negative)	2
30	Snook, Davidson, Butler, et al., 2014	Newtonian Matrix Suspensions	nL^2d=1.5–3 polyamide rod-like particles or fibres with aspect ratios 12, 13, 17 and 32 in water (10.2 wt%), Triton X-100 (78.0 wt%), and zinc chloride (11.8 wt%).	TT & RC	~0.5	2

31	Zarraga et al., 2000	Newtonian Matrix Suspensions	30-55% glass spheres with 43 and 73.6 μm average diameters in 98 wt% glycerin mixture with water (GW) and 70% corn syrup and 30% glycerin (KG)	CPDT & RC	~ -3.6 (Both negative)	2
32	Ohl and Gleissle, 1992	Polymer solution	pure polyisobutene	CPD_T	0.1 ± 0.1	1
		Viscoelastic Matrix Suspension	34.5% limestone with a mean particle diameter of 9 μm in polyisobutene		1 to 3	
33	Mall-Gleissle et al., 2002	Viscoelastic Matrix Suspensions	0-25% sieved glass beads of 0.5 and 4 μm average diameter in Silicone oil matrix	$CP\text{-}PP_T$ with guard-ring	0.1 to 0.7	2
34	Haleem and Nott, 2009	Viscoelastic Matrix Suspensions	0-40% monodisperse spheres of poly methylmethacrylate, PMMA with 8 μm average diameter in polyacrylamide-co-acrylic acid of average molecular weight 5*10^6 and of weight fraction 1.5*10^−2 in a mixture of 74.5% glycerol and 25.5% water (by weight)	$CP\text{-}PP_T$	0.62	2
35	Lin et al., 2014	Viscoelastic Matrix Suspensions	15-49% glass spheres of average diameter 3.35 μm, in a silicon oil [polydimethylsiloxane (PDMS)]	$CP\text{-}PP_T$	0.25 to 5	2
36	Zarraga et al., 2001	Viscoelastic Matrix Suspensions	30-53% glass spheres with 43 μm average diameters in 0.015% polyacrylamide (by weight) solution in a Newtonian fluid composed of a 79.4/19.8/0.7 by weight mixture of corn syrup, glycerin, and water	CP-PPT & RC	0.1 to 1.6	2

*Note

$CP\text{-}PP_T$	CP_PP_Thrust	CP_G	C_P Pressure gradient	RC	Rod climbing	CR	C_Ring
CPD_T	CP_Distance	CPP	C_Partitioned Plate	TT	Tilted Trough	PR	P_Ring

Table 2: Low and high shear rate asymptotic predictions for common viscoelastic models ($\lambda_2 = (\eta_2/\eta_0)\lambda_1, \beta = \eta_2/\eta$).
For Giesekus, PTT and JS $\lambda_2 = \eta_2 = 0$ and therefore $\lambda_1 = \lambda$ and $\eta_0 = \eta_1 = \eta$

Model		$\eta(\dot{\gamma})$	$N_1(\dot{\gamma})$	$-N_2(\dot{\gamma})$	$\frac{N_1(\dot{\gamma})}{\tau_{xy}} = \frac{N_1(\dot{\gamma})}{\eta(\dot{\gamma})\dot{\gamma}}$	$\frac{-N_2(\dot{\gamma})}{N_1(\dot{\gamma})}$
Oldroyd-A		η_0	$2\eta_0(\lambda_1 - \lambda_2)\dot{\gamma}^2$	$2\eta_0(\lambda_1 - \lambda_2)\dot{\gamma}^2$	$2(1-\beta)\lambda_1\dot{\gamma}$	1
Oldroyd-B		η_0	$2\eta_0(\lambda_1 - \lambda_2)\dot{\gamma}^2$	0	$2(1-\beta)\lambda_1\dot{\gamma}$	0
co-rot Oldroyd	$(\dot{\gamma} \to 0)$	$\eta_0 = \eta_1 + \eta_2$	$2\eta_0(\lambda_1 - \lambda_2)\dot{\gamma}^2$	$\eta_0(\lambda_1 - \lambda_2)\dot{\gamma}^2$	$2(1-\beta)\lambda_1\dot{\gamma}$	$\frac{1}{2}$
	$(\dot{\gamma} \to \infty)$	η_2	$\frac{\eta_1}{\lambda_1}$	$\frac{\eta_1}{2\lambda_1}$	$\frac{\eta_1}{\eta_2}\frac{1}{\lambda_1\dot{\gamma}}$	$\frac{1}{2}$
Giesekus $(\lambda_2 = 0)$	$(\dot{\gamma} \to 0)$	η	$2\eta\lambda\dot{\gamma}^2$	$\alpha\eta\lambda\dot{\gamma}^2$	$2(1-\beta)\lambda\dot{\gamma}$	$\frac{\alpha}{2}$
	$(\dot{\gamma} \to \infty)$	$\sqrt{\frac{(1-\alpha)}{\alpha}}\frac{\eta}{\lambda\dot{\gamma}}$	$\frac{\sqrt{2}}{\alpha}\left(\alpha(1-\alpha)\right)^{1/4}\eta(\frac{\dot{\gamma}}{\lambda})^{1/2}$	$\frac{\eta}{\lambda}$	$\frac{\sqrt{2\alpha}\left(\alpha(1-\alpha)\right)^{1/4}}{\alpha\sqrt{(1-\alpha)}}(\lambda\dot{\gamma})^{1/2}$	$\to 0$
PTT & Johnson-Segalman (a=ξ) $(\lambda_2 = 0)$	$(\dot{\gamma} \to 0)$	η	$2\eta\lambda\dot{\gamma}^2$	$a\eta\lambda\dot{\gamma}^2 = \frac{aN_1}{2}$	$2\lambda\dot{\gamma}$	$\frac{a}{2}$
	JS (PTT $\varepsilon \to 0$) $(\dot{\gamma} \to \infty)$	$\frac{\eta}{2a\left(1-\frac{a}{2}\right)(\lambda\dot{\gamma})^2}$	$\frac{\eta}{a\left(1-\frac{a}{2}\right)\lambda}$	$\frac{\eta}{2\left(1-\frac{a}{2}\right)\lambda} = \frac{aN_1}{2}$	$2\lambda\dot{\gamma}$	$\frac{a}{2}$
	PTT $(\dot{\gamma} \to \infty)$	$\frac{(1+\varepsilon/\xi)\eta}{2\xi\left(1-\frac{\xi}{2}\right)(\lambda\dot{\gamma})^2}$	$\frac{\eta}{\xi\left(1-\frac{\xi}{2}\right)\lambda}$	$\frac{\eta}{2\left(1-\frac{\xi}{2}\right)\lambda} = \frac{\xi N_1}{2}$	$\frac{2\lambda\dot{\gamma}}{(1+\varepsilon/\xi)}$	$\frac{\xi}{2}$

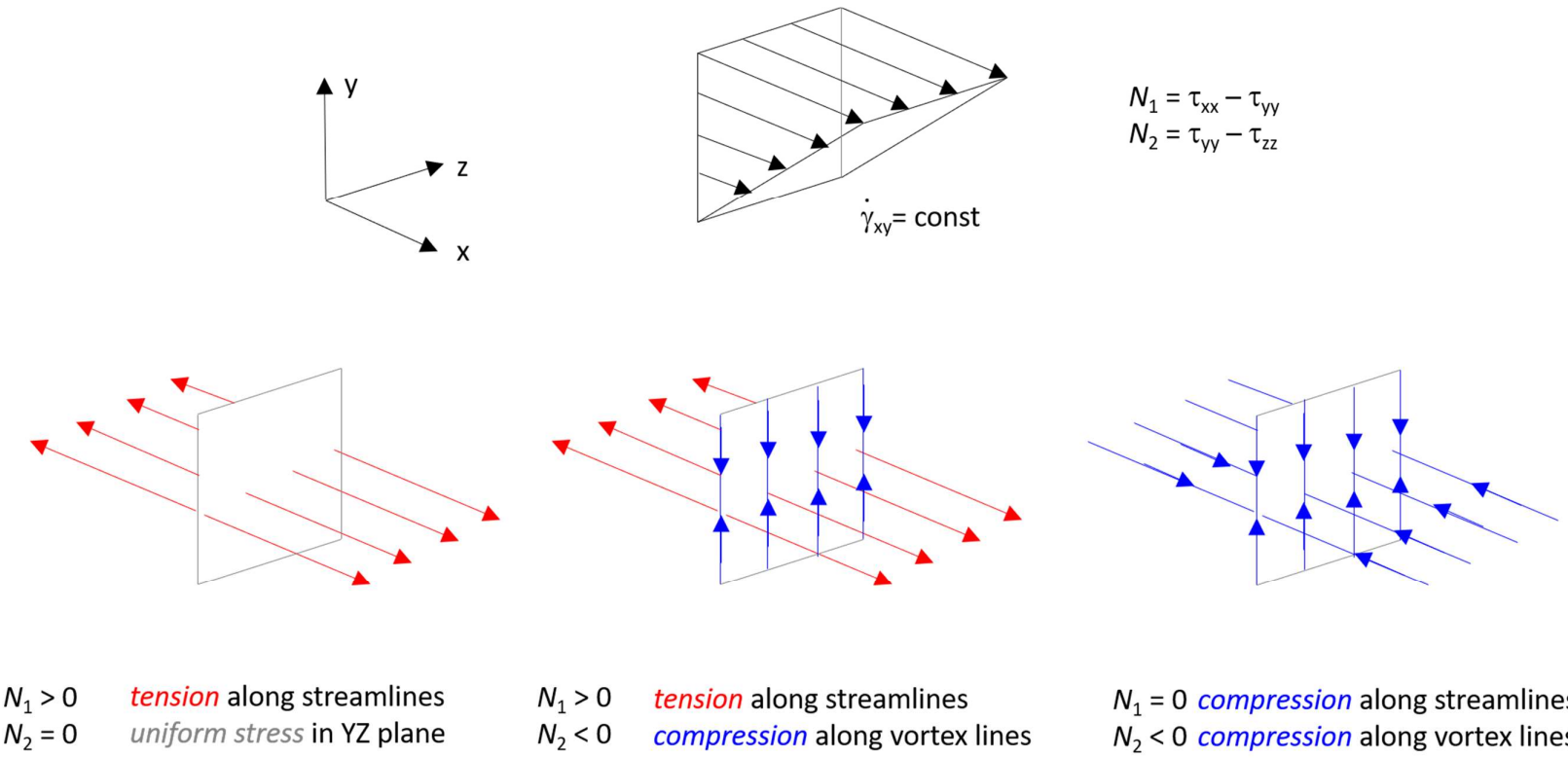

Figure 1. A cartoon illustrating how various configurations of the first and second normal-stress differences create tension or compression in a fluid element along streamlines and vortex lines in a homogeneous shear flow in a Cartesian coordinate system. Top row left to right: Cartesian coordinate system; schematic of homogeneous shear flow in the XY plane; definitions of N_1 and N_2 in this coordinate system. Bottom row: Left- tension along the streamlines (parallel to the velocity vector) in a shear flow for a complex fluid with positive N_1 and vanishing N_2 typical of dilute polymeric fluid with uniform stress in perpendicular plane; Middle- tension along streamlines and compression along vortex lines (i.e. lines tangential to the velocity vector) in a shear flow for a complex fluid with positive N_1 and negative N_2 typical of concentrated polymeric solutions and melts; Right- compression along both streamlines and vortex lines in a shear flow for a hypothetical dense suspension with N_1 ~0 and negative N_2 . For all cases, analysis assumes $\tau_{zz}=0$ and $N_1 \neq -N_2$. Note, as the isotropic pressure is an undetermined constant, it is possible to obtain, different, yet equivalent distributions. In the right-hand case if $\tau_{zz}>0$ and $\tau_{xx}=\tau_{yy}=0$ (so $N_1=0$ and N_2 =-ve) this would be uniform stress in streamlines and vortex lines and a tension in the vorticity (z) direction.

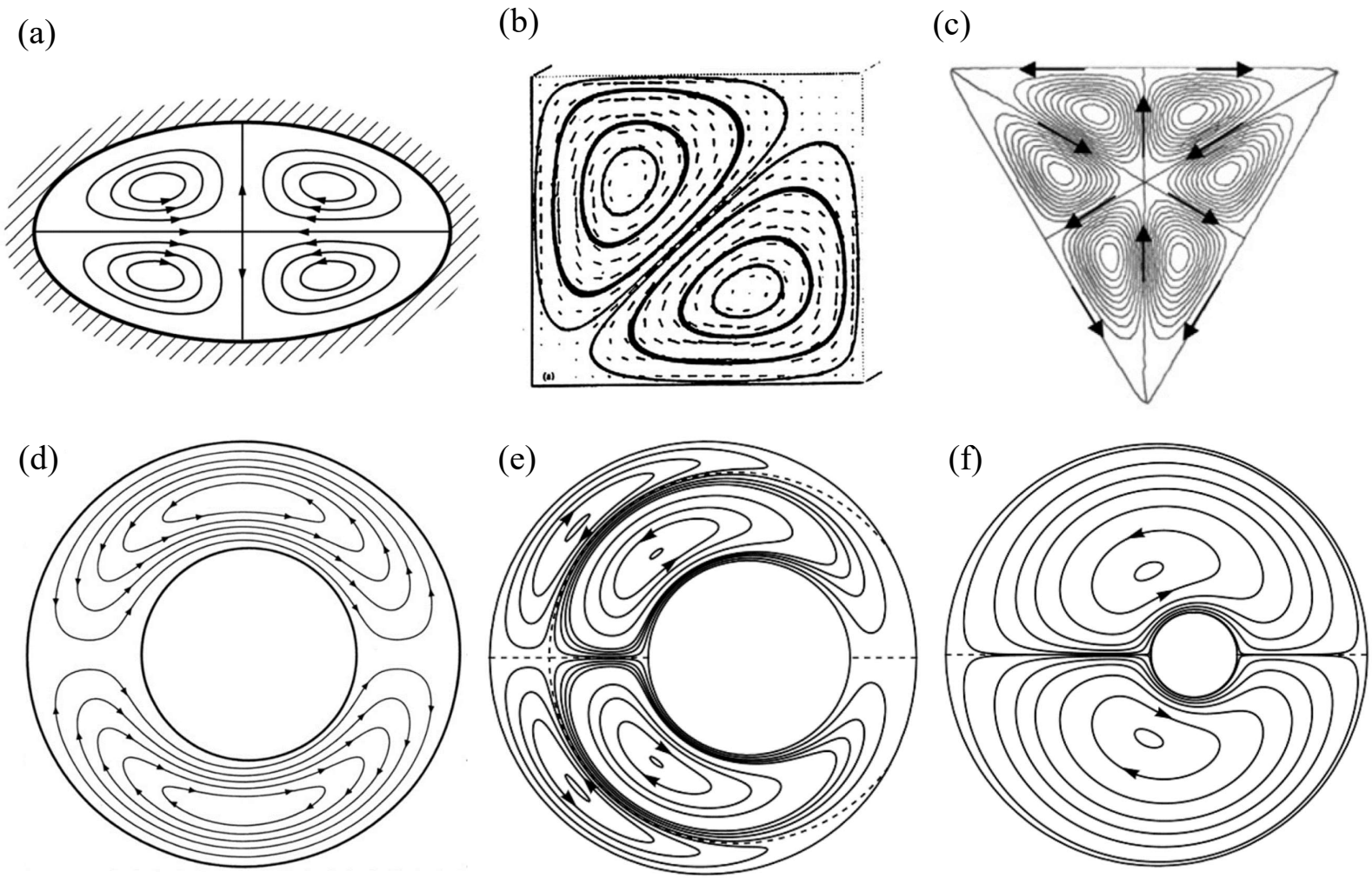

Figure 2: Different results from the literature for secondary flows driven by gradients of N_2 taking complex forms for different cross-sections and boundary conditions. (a) Elliptic cross-section (Green and Rivlin, 1956), (b) bottom left quadrant of a square (Townsend, et al., 1976), (c) triangular (Letelier, et al., 2002) and (d, e, f) "almost" concentric – the eccentricity is used as a perturbation parameter (Mollica and Rajagopal, 1999) and eccentric annulus (Letelier, et al., 2019)

(a) (b)

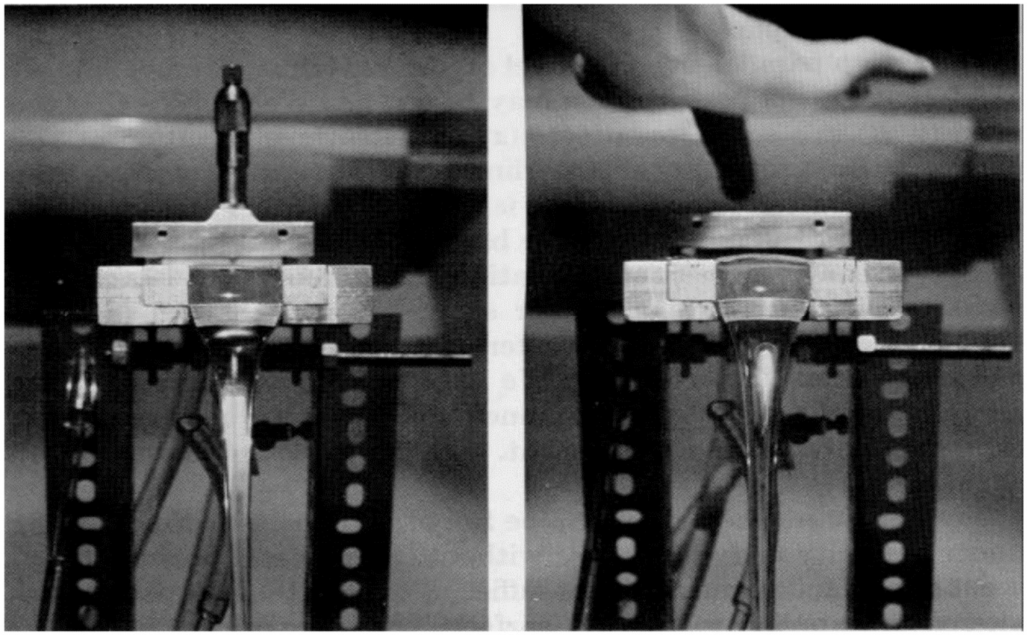

Figure 3: Photographs of free surface profiles in rectangular open channel: (a) 3 Pa.s silicone oil, flat surface; (b) 6.8% polyisobutylene/cetane solution showing convex profile (Tanner, 1970).

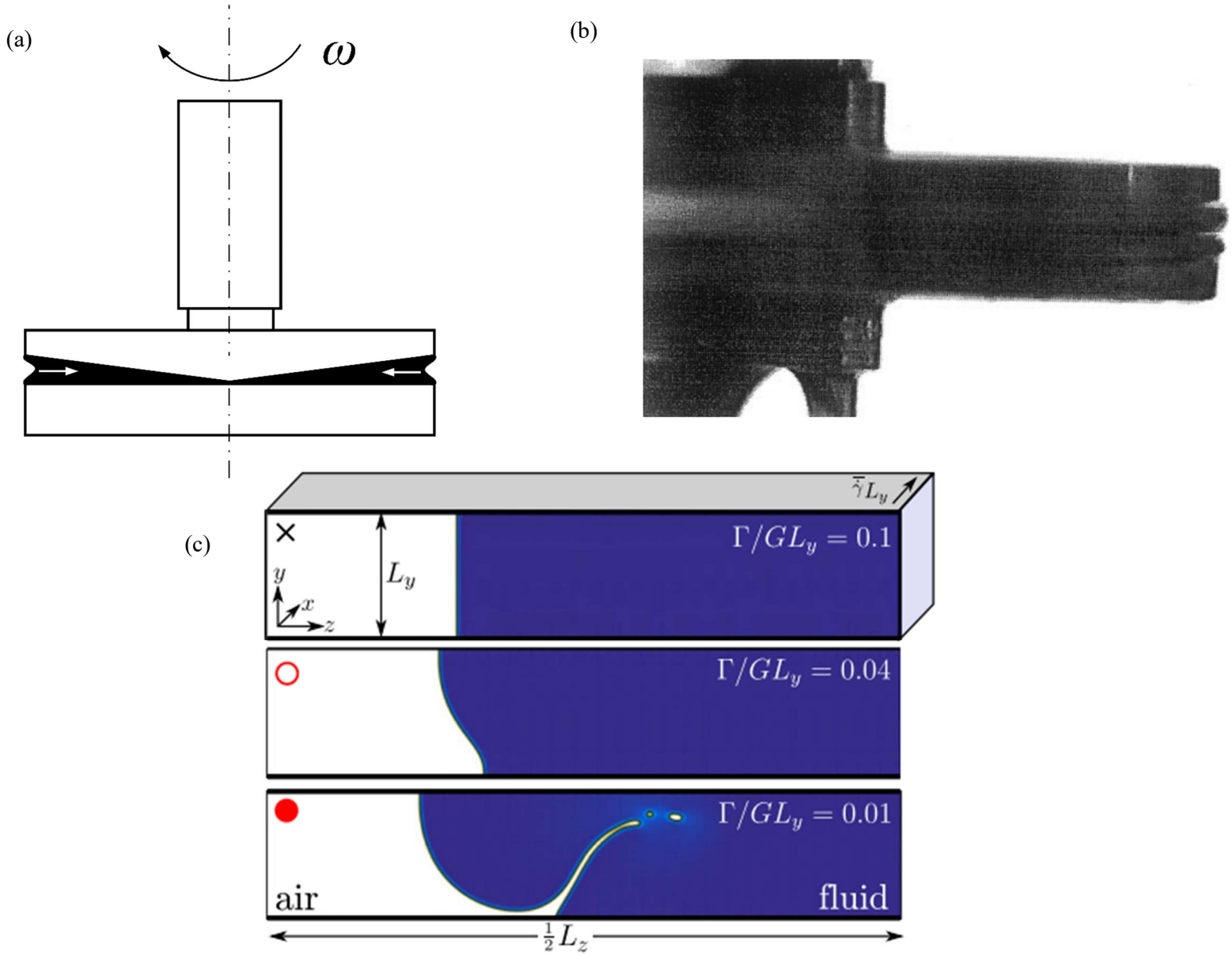

Figure 4: (a) Schematic diagram showing “edge” or “shear” fracture in a cone-and-plate rheometer, (b) Experimental photograph for Minty Gel toothpaste in the cone-and-plate rheometer (Keentok and Xue, 1999), and (c) Snapshots from full nonlinear simulations of the Giesekus model between hard walls (Hemingway, Kusumaatmaja, and Fielding, 2017).

(a)

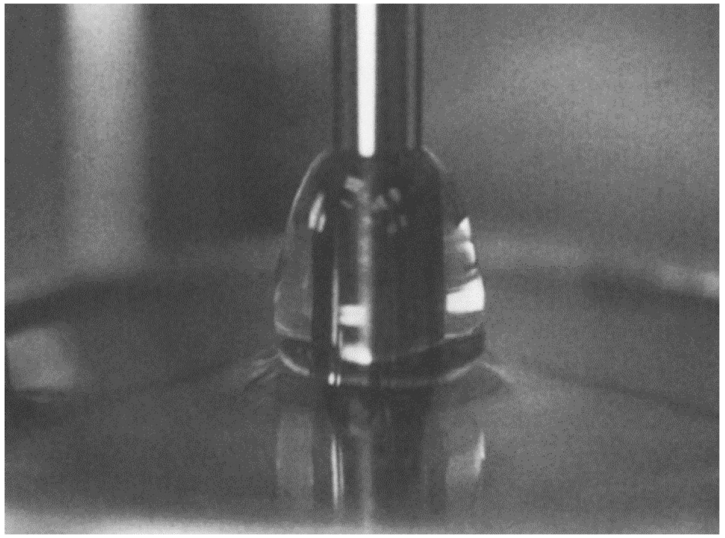

(b)

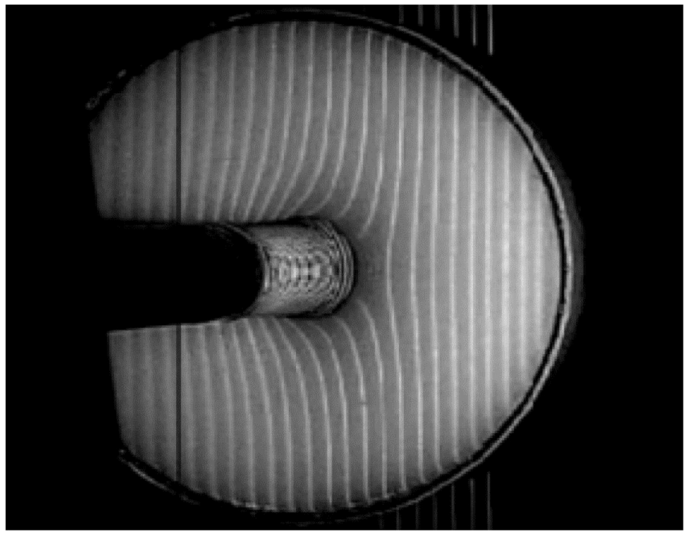

Figure 5: (a) Photograph of rod-climbing effect in test fluid M1 - Boger fluid (Hu et al., 1990), and (b) is a typical image of the free surface deflection of rod dipping in a concentrated suspension viewed from above (Boyer et al., 2011).

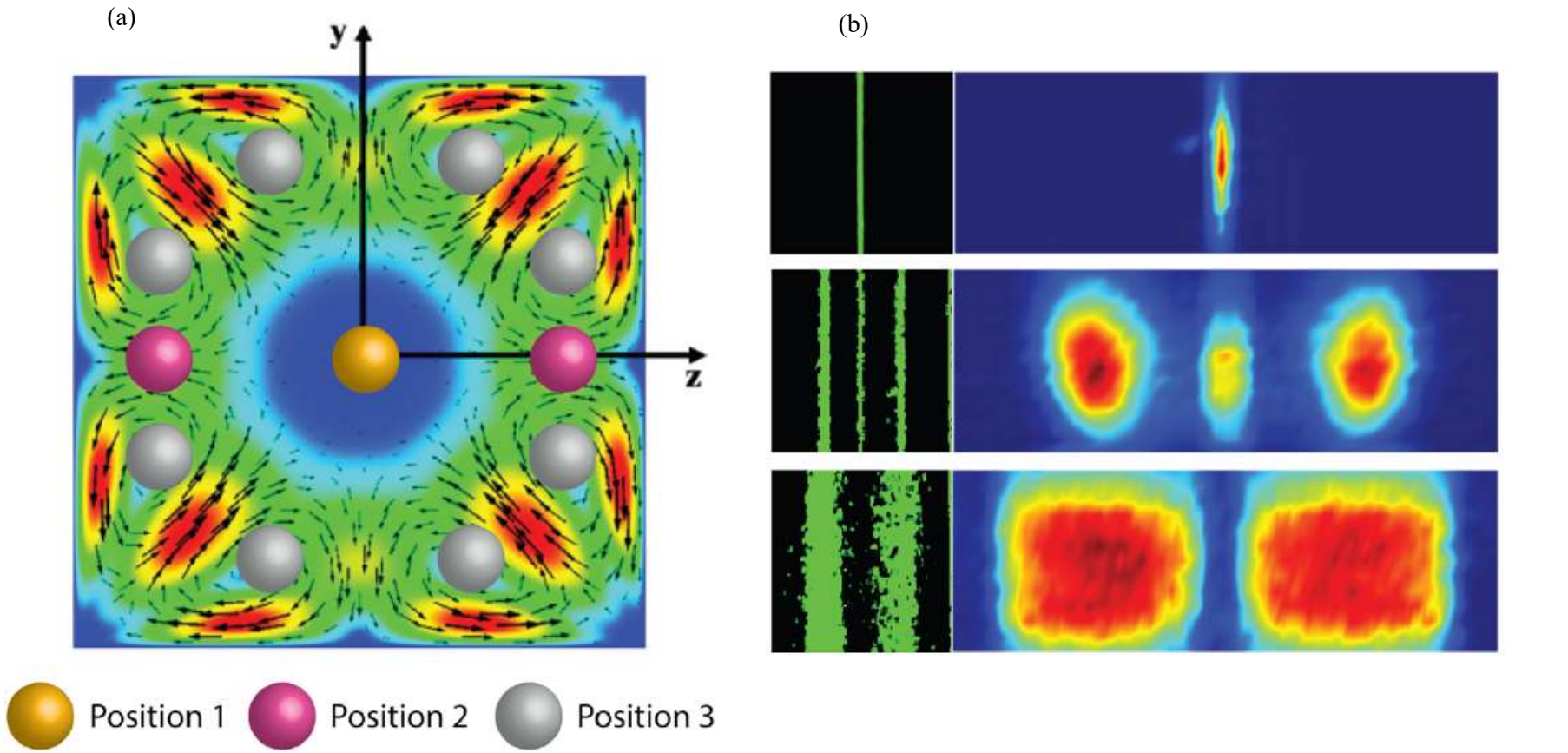

Figure 6: (a) Theoretical predictions for secondary flows in noncircular channels induced by the second normal-stress difference (Villone, D'Avino, Hulsen, et al., 2013) and spheres represent the balance positions in the channel cross section (Feng, et al., 2019), and (b) Particle distributions at a microfluidics channel exit observed in the study by Feng, et al., 2019 for 3 μm beads in a 5 mg/ml PEO solution at the following flow rates: 5 μl/min (top); 10 μl/min (middle); 50 μl/min (bottom).

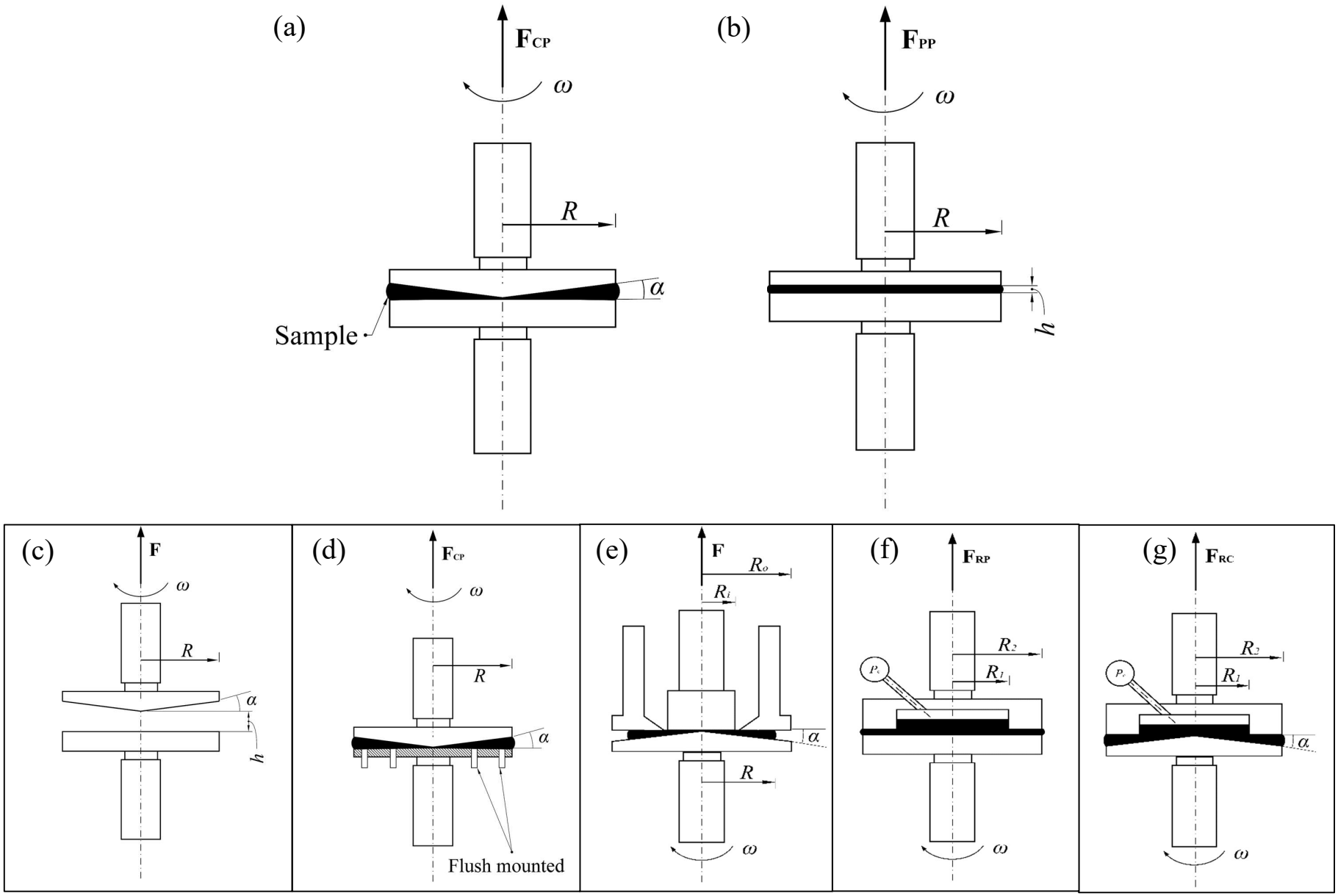

Figure 7: Schematic diagrams of the rotational rheometry techniques to measure normal-stress differences. (a) Cone-and-plate rheometry, (b) parallel-plate geometry, (c) cone-and-plate with distance adjustment, (d) cone-and-plate with pressure distribution measurement, (e) cone-and-partitioned plate, (f) plate-and-ring geometry, and (g) cone-and-ring geometry

)

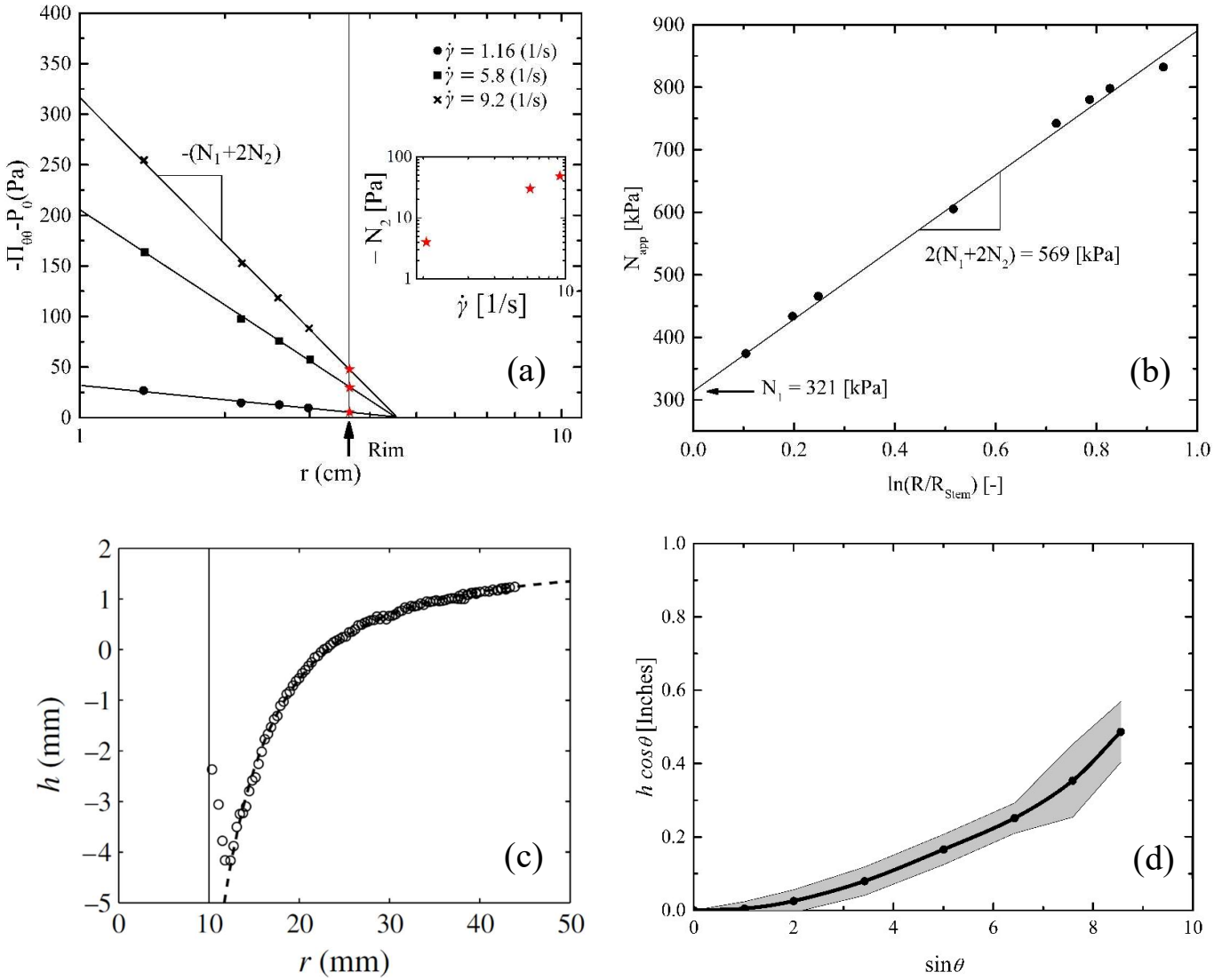

Figure 8: (a) Net vertical pressure force as a function of radial position in cone-and-plate rheometer for NIST rheology standard, inset plot is N_2 values at the cone rim (Magda et al., 1991b), (b) determination of the first (N_1) and second (N_2) normal-stress difference using cone-and-partitioned plate for different samples with different sizes (Schweizer, 2002), (c) experimental profile (o) computed from the processed image of a suspension free surface deflection and theoretical profile $h(r) = -h_0 \frac{{R_1}^2}{r^2} + h_1$ (dashed line) neglecting surface tension and inertia. The vertical solid line refers to the rod radius. (Boyer et al., 2011), and (d) is the vertical component of the central free surface rise as a function of the channel tilt angle and measurement error shown in grey (Tanner, 1970).

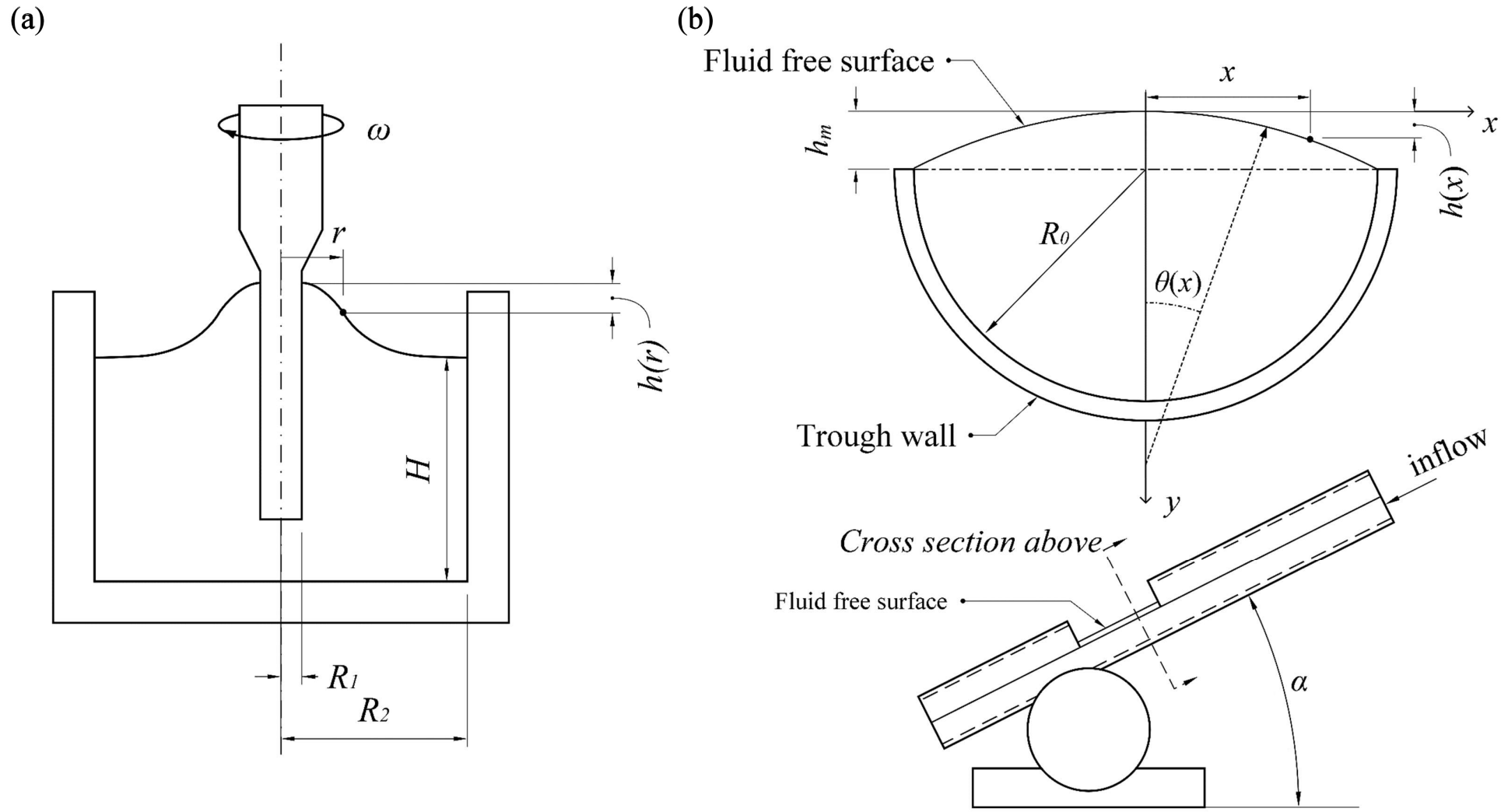

Figure 9: Schematic diagram of the surface deflection rheometry techniques to measure normal-stress differences. (a) Rod climbing (Weissenberg effect) (Magda et al., 1991), and (b) Tilted trough experiment (Dai, Qi, and Tanner, 2014 & Kuo and Tanner, 1974)

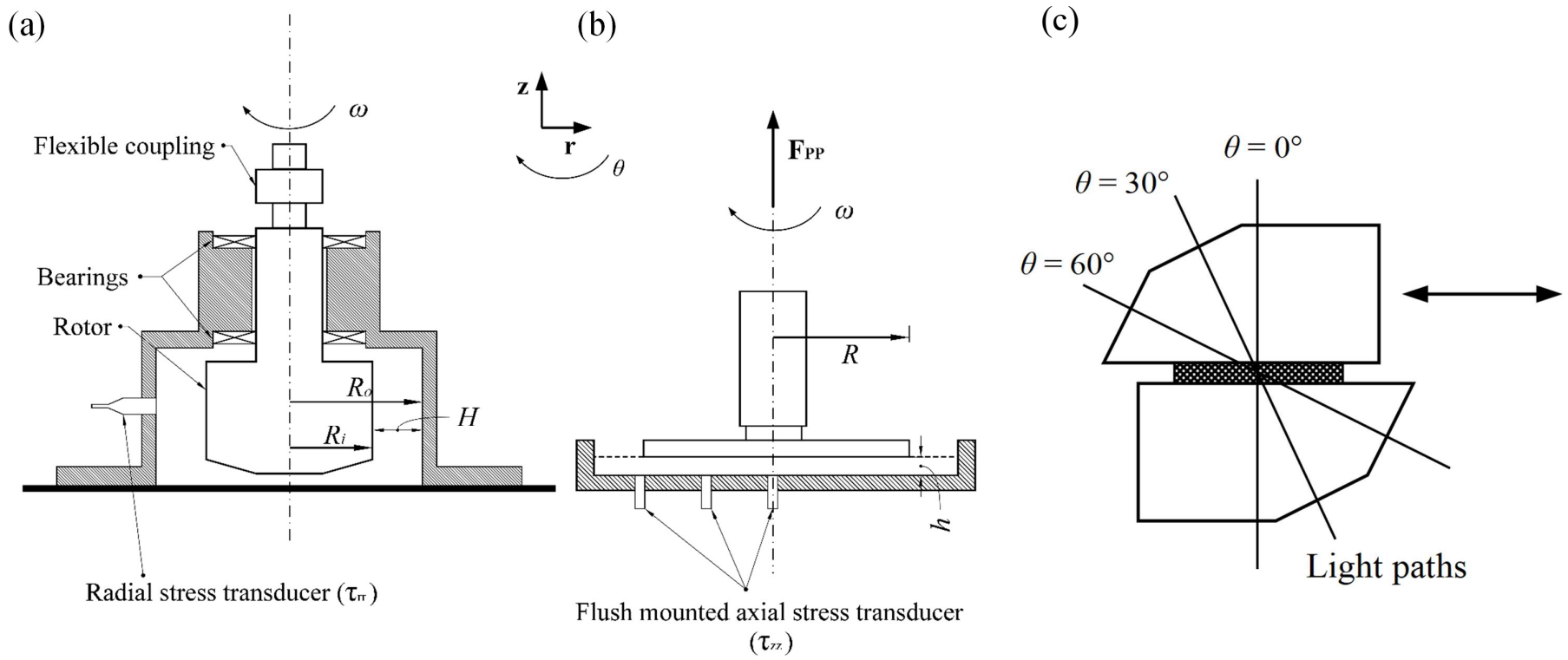

Figure 10: Schematic diagram of (a), (b) the cylindrical Couette flow technique to measure normal-stress differences by measuring the radial and axial normal-stresses (Singh and Nott, 2003), and (c) Flow birefringence optical method (Brown et al., 1995)

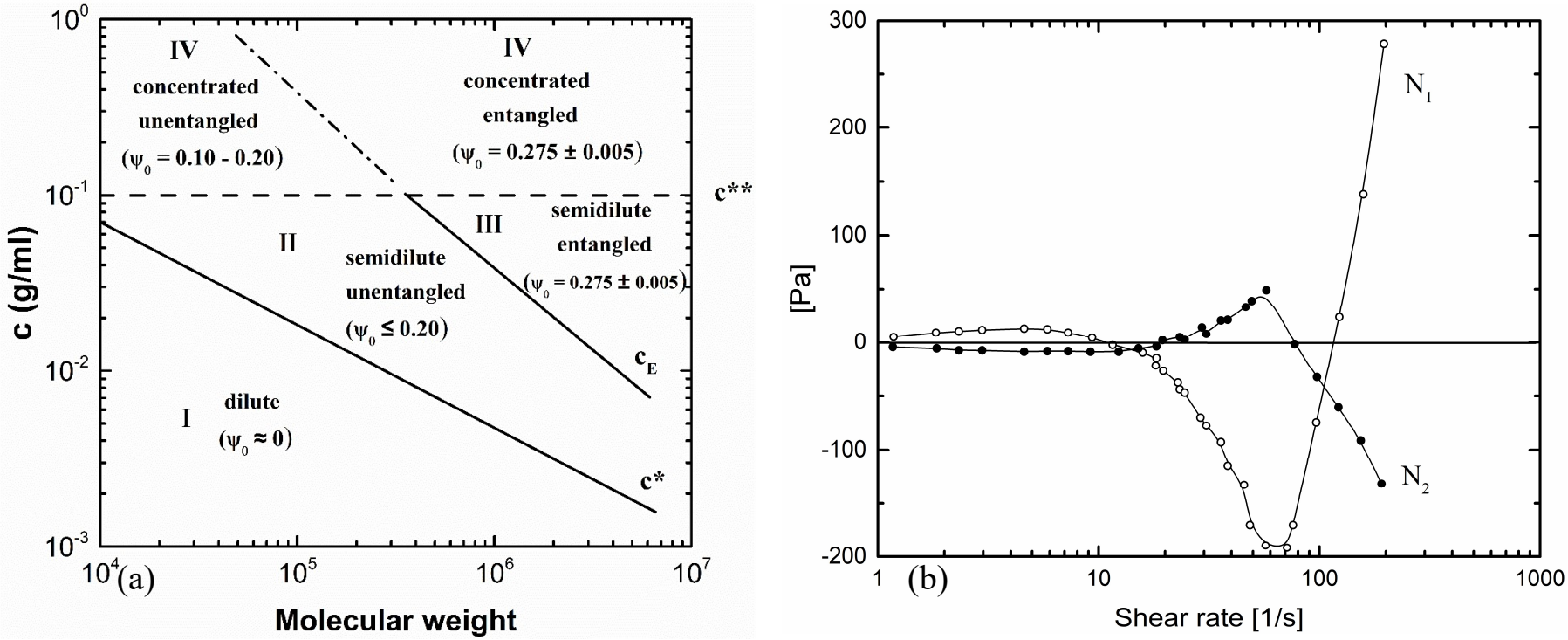

Figure 11: (a) The approximate monodisperse polystyrene concentration and entanglement regime with measured values of the zero-shear rate normal-stress differences ratio in parentheses, using (CP_G method) (Magda and Baek, 1994), and (b) is the first and second normal-stress differences measured for 12.5% PBLG solution (fully liquid crystalline) (Magda et al., 1991a).

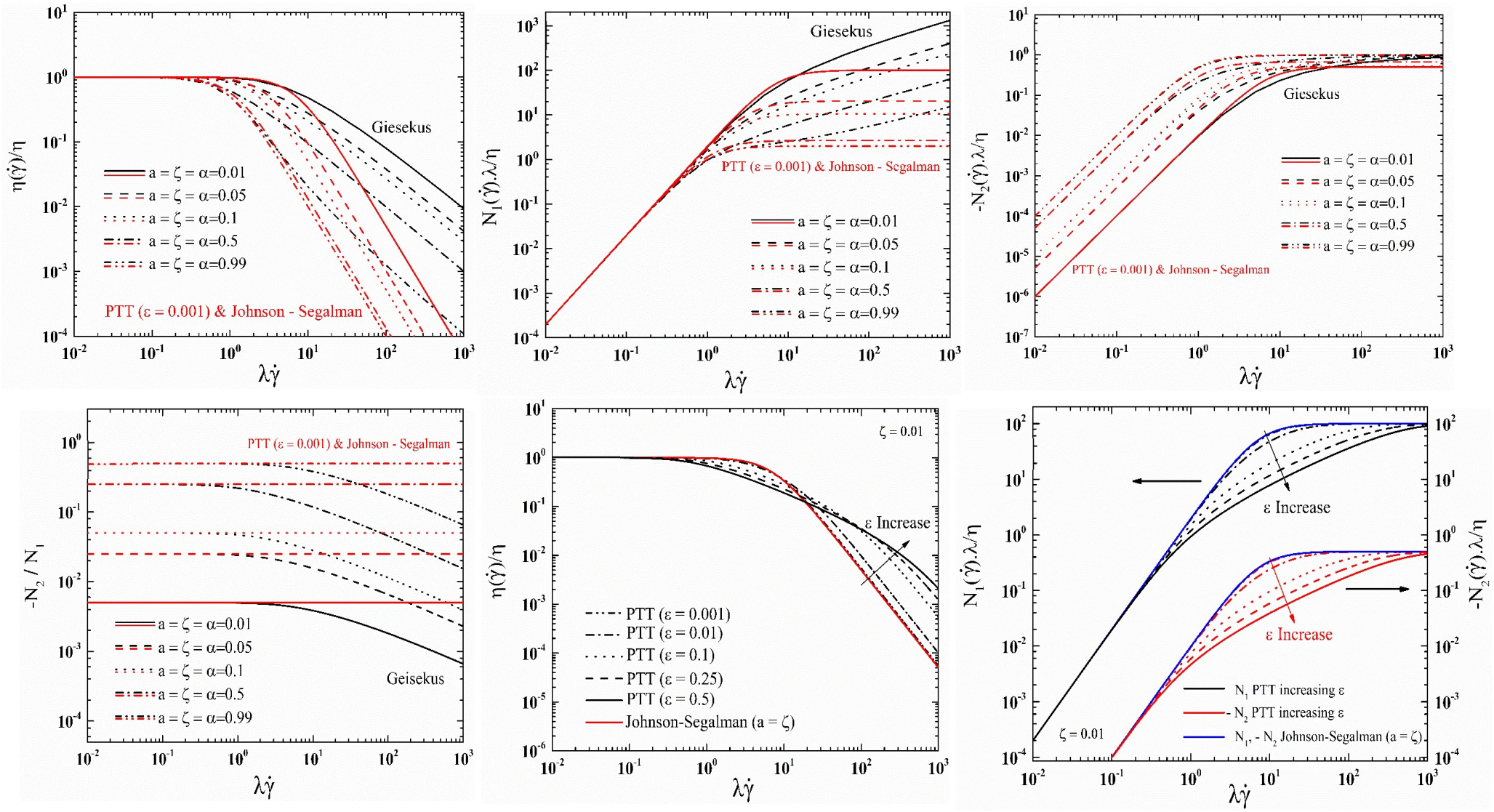

Figure 12: (a, b, c, d) Giesekus model prediction for normalised viscosity, normalised first normal-stress difference N_1, normalised second normal-stress difference N_2, and the ratio $(-N_2/N_1)$ and comparison with Full Phan-Thien Tanner (PTT) and Johnson-Segalman model predictions for the same normalised rheological functions. (e) and (f) show the effect of changing ε on the same normalised rheological functions.